NASA TN D-2623

EFFECT OF FIN-FLARE COMBINATIONS ON THE AERODYNAMIC CHARACTERISTICS OF A BODY AT MACH NUMBERS 1.61 AND 2.20

By Clyde Hayes and Roger H. Fournier

Langley Research Center
Langley Station, Hampton, Va.

NATIONAL AERONAUTICS AND SPACE ADMINISTRATION

For sale by the Office of Technical Services, Department of Commerce,
Washington, D.C. 20230 -- Price $2.00

EFFECT OF FIN-FLARE COMBINATIONS ON THE AERODYNAMIC CHARACTERISTICS OF A BODY AT MACH NUMBERS 1.61 AND 2.20

By Clyde Hayes and Roger H. Fournier
Langley Research Center

SUMMARY

16578

An investigation has been conducted in the Langley 4- by 4-foot supersonic pressure tunnel at Mach numbers of 1.61 and 2.20 to determine the effectiveness of various combinations of fins and flares in stabilizing a cone-cylinder missile configuration having a fineness ratio of 10.

An increase in either fin or flare angle led to significant increases in the normal-force-curve slope and the stability level and a small increase in axial force due to the fins but a rather large increase in axial force due to the flares. The addition of flares to the model with 1/6 body length fins had little effect on the normal-force-curve slope and the stability level until the flare angle became sufficiently steep to cause flow separation forward of the flare-body juncture. The resulting flow separation caused an increase in the normal-force-curve slope and in stability level. The addition of flares to the model with 5/12 body length fins generally resulted in a slight decrease in the normal-force-curve slope and stability level.

AUTHOR

INTRODUCTION

The design of missile configurations is a continuing effort which involves wind-tunnel tests, flight tests, and theoretical studies of various vehicles. Aerodynamic lift and stabilization of these vehicles is generally provided by means of either fins or flared afterbodies, depending upon various aerodynamic and structural requirements. Examples of research on flared-afterbody configurations may be found in references 1 and 2, and a comparison of fin and flare effectiveness may be found in reference 3. Occasionally, missiles equipped with either a flare or a fin have required additional lift and stability, and the question arises whether a flare could be added between fins or fins added to a flare to augment the lift and stability characteristics. Theoretical calculations of such conditions are limited because of mutual fin-flare interference effects, and test results to date have been inconclusive as to combined effects.

An investigation was performed in the Langley 4- by 4-foot supersonic pressure tunnel to determine the effectiveness of various fin-flare combinations on the longitudinal aerodynamic characteristics of a cone-cylinder configuration having a fineness ratio of 10. The configurations included flares and fins of 1/6 and 5/12 body length with fin and flare angles from 0° to 27.8°. Although the basic configurations had fins and flares of equal lengths with the span of the fins varying, several additional configurations were tested in which the fin and flare spans were kept equal and the lengths of the fins were varied, and thus low-aspect-ratio fins were obtained.

The investigation was performed at Mach numbers of 1.61 and 2.20, through an angle-of-attack range from about -4° to 14° at a sideslip angle of 0°. The Reynolds number for this investigation was 2.5×10^6 per foot.

SYMBOLS

The coefficients of forces and moments are referred to the body axis system with aerodynamic moments taken about a point 12.00 inches forward of the base of each test configuration. Symbols are defined as follows:

A	cross-sectional area of basic body, sq ft
C_A	axial-force coefficient, Axial force/qA
$C_{A,\alpha=0^\circ}$	axial-force coefficient at $\alpha = 0^\circ$
$C_{A,b}$	base axial-force coefficient, Base axial force/qA
C_m	pitching-moment coefficient, Pitching moment/qAD
C_{m_α}	slope of pitching-moment curve at $\alpha = 0^\circ$, per deg
C_N	normal-force coefficient, Normal force/qA
C_{N_α}	slope of normal-force curve at $\alpha = 0^\circ$, per deg
D	diameter of basic body, in.
d_{flare}	flare diameter, in.
d_{fin}	fin span, in.
l	length of fin or flare, in.
M	free-stream Mach number
q	free-stream dynamic pressure, psf

r	radius of model tip, in.
α	angle of attack of body center line, deg
θ	angle of fin with respect to body center line, deg
ϕ	angle of flare with respect to body center line, deg

APPARATUS AND METHODS

Tunnel

The investigation was performed in the Langley 4- by 4-foot supersonic pressure tunnel, which is a variable-pressure continuous-flow type. Flexible walls on the nozzle leading to the test section permit changes in tunnel Mach number at discrete intervals between 1.41 and 2.20.

Test Conditions

The investigation was performed at Mach numbers of 1.61 and 2.20 with total pressures of 8.85 and 11.20 pounds per square inch, respectively, corresponding to a Reynolds number of 2.5×10^6 per foot. The angle of attack was varied from about -4° to 14° for an angle of sideslip of 0°. The dewpoint for both Mach numbers was maintained below -25° F in order to assure negligible condensation effects, and the tunnel stagnation temperature was held constant at 110° F.

A 1/16-inch-wide transition strip with No. 60 carborundum grains imbedded in plastic was affixed around the model nose 1 inch aft of the tip to assure turbulent flow over the models.

Models

The basic model was the same as the one used for the tests of reference 1. A drawing with dimensional details of the basic body, the fins, and the flares is presented as figure 1. The model was composed of a conical forebody 1/3 of the body length with a rounded tip, and a cylindrical afterbody. Two lengths of fins and flares were used with the basic body, one equal to 1/6 body length (designated as short fin or flare), the other equal to 5/12 body length (designated as long fin or flare). For the short fin-flare family, fins with angles of 10°, 19.3°, and 27.8° from the model center line were provided with flares with angles of 5°, 10°, 19.3°, and 27.8° that could be inserted between the fins. The fins for the long fin-flare family had angles of 5°, 7.5°, 10°, and 12.1° used in conjunction with flares of 2.5°, 5°, 7.5°, 10°, and 12.1°. In addition to these two families of fins and flares, three fins with low aspect ratios were used in combination with short flares, and one fin was used with the long flare. These fins with low aspect ratios had spans equal to the

flare diameter and had exposed areas equal to the areas of some of the fins of the basic families.

Measurements, Corrections, and Accuracy

Aerodynamic forces and moments were measured with a sting-supported six-component, electrical, strain-gage balance housed within the model. Base pressure was measured for each configuration by means of a single static orifice located in the balance chamber cavity.

Angles of attack have been corrected for deflection of the balance-sting combination due to aerodynamic loads. In addition, the axial-force-coefficient data have been adjusted to correspond to free-stream static pressure acting on the base of the model. The magnitudes of the base axial-force coefficients used in adjusting these data may be found in figure 2.

The accuracy of the individually measured quantities, based on calibration and repeatability of data, is estimated to be within the following limits:

C_A	±0.01
C_m	±0.02
C_N	±0.03
M	±0.01
α, deg	±0.10

PRESENTATION OF RESULTS

The results are presented in the following manner:

	Figure
Basic body alone, M = 1.61 and 2.20	3
Basic fin-flare configurations:	
Short fin-flare, $\theta = 10^\circ$, M = 1.61	4(a)
Short fin-flare, $\theta = 10^\circ$, M = 2.20	4(b)
Short fin-flare, $\theta = 19.3^\circ$, M = 1.61	4(c)
Short fin-flare, $\theta = 19.3^\circ$, M = 2.20	4(d)
Short fin-flare, $\theta = 27.8^\circ$, M = 1.61	4(e)
Short fin-flare, $\theta = 27.8^\circ$, M = 2.20	4(f)
Long fin-flare, $\theta = 5^\circ$, M = 1.61	4(g)
Long fin-flare, $\theta = 5^\circ$, M = 2.20	4(h)
Long fin-flare, $\theta = 7.5^\circ$, M = 1.61	4(i)
Long fin-flare, $\theta = 7.5^\circ$, M = 2.20	4(j)
Long fin-flare, $\theta = 10^\circ$, M = 1.61	4(k)
Long fin-flare, $\theta = 10^\circ$, M = 2.20	4(l)
Long fin-flare, $\theta = 12.1^\circ$, M = 1.61	4(m)
Long fin-flare, $\theta = 12.1^\circ$, M = 2.20	4(n)

DISCUSSION OF RESULTS

The longitudinal aerodynamic characteristics for the basic body alone are presented in figure 3 for both Mach numbers. The basic data for both the short and the long fin-flare configurations are presented in figure 4. These results are summarized in figure 5 where the parameters C_{m_α}, C_{N_α}, and $C_{A,\alpha=0^\circ}$ are presented as functions of flare angle for various constant fin angles. Data showing the effectiveness of the flare with no fins ($\phi = \theta$) indicate that an increase in flare angle results in an increase in C_{N_α} and an increase in stability ($-C_{m_\alpha}$), but these increases occur at the expense of a large increase in $C_{A,\alpha=0^\circ}$. The sharp increase in effectiveness of the flare, in particular for flare angles above about 20°, is probably due to flow separation forward of the flare. (See ref. 1.)

For the configuration with only fins ($\phi = 0^\circ$), a progressive increase in the fin angle results in increases in both C_{N_α} and stability, but very little increase in $C_{A,\alpha=0^\circ}$. The addition of fins at any flare angle provides an increment in C_{N_α} and $-C_{m_\alpha}$ until the fin angle equals the flare angle. The addition of a flare for a constant fin angle generally has little effect on the level of C_{N_α} or C_{m_α} for the short-flare configurations; thus, the increase in effectiveness of the flare essentially compensates for a decrease in effectiveness of the fin. (See figs. 5(a) and 5(b).) However, for the long fin-flare configurations (figs. 5(c) and 5(d)), the addition of the flare at a constant fin angle results in a decrease in C_{N_α} and in stability; thus, the fin effectiveness for the long fin decreases more rapidly than the flare effectiveness increases.

Three of the short flare and one of the long flare configurations were also tested to determine some effects of fin aspect ratio on the aerodynamic characteristics of fin-flare configurations. The fins had exposed areas equal to some of those previously discussed, but had lower aspect ratios (fin span equal to flare diameter). The results of these tests are presented in figure 6,

and the flares with the fins of high aspect ratios are presented for comparison. As might be expected, the flare configurations in combination with the fins of high aspect ratio produced the greater values of normal-force coefficient and were more stable than the comparable configurations with the fins of low aspect ratio.

CONCLUSIONS

An investigation has been conducted at Mach numbers of 1.61 and 2.20 to determine the effectiveness of fin-flare combinations of 1/6 and 5/12 body length in stabilizing a cone-cylinder missile configuration having a fineness ratio of 10. The results indicated the following:

1. An increase in either fin or flare angle led to significant increases in the normal-force-curve slope and the stability level, and a small increase in axial force due to the fins but a rather large increase in axial force due to the flares.

2. The addition of flares to the model with 1/6 body length fins had little effect on the normal-force-curve slope and the stability level until the flare angle became sufficiently steep to cause flow separation forward of the flare-body juncture. The resulting flow separation caused an increase in the normal-force-curve slope and in stability level.

3. The addition of flares to the model with 5/12 body length fins generally resulted in a slight decrease in the normal-force-curve slope and stability level.

Langley Research Center,
National Aeronautics and Space Administration,
Langley Station, Hampton, Va., November 18, 1964.

REFERENCES

1. Carraway, Ausley B.; Turner, Kenneth L.; and Crowder, Janette M.: Effects of Afterbody Shape on the Aerodynamic Characteristics of a Fineness-Ratio-10 Cone-Cylinder Configuration at Mach Numbers From 1.57 to 4.65 Including Design Parameter Curves for Circular Afterbody Flares. NASA TM X-348, 1960.

2. Kirk, Donn B.; and Chapman, Gary T.: The Stabilizing Effectiveness of Conical Flares on Bodies With Conical Noses. NASA TM X-30, 1959.

3. Jorgensen, Leland H.; Spahr, J. Richard; and Hill, William A., Jr.: Comparison of the Effectiveness of Flares With That of Fins for Stabilizing Low-Fineness-Ratio Bodies at Mach Numbers From 0.6 to 5.8. NASA TM X-653, 1962.

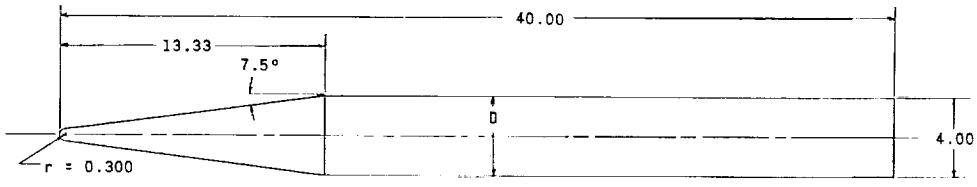

Basic body

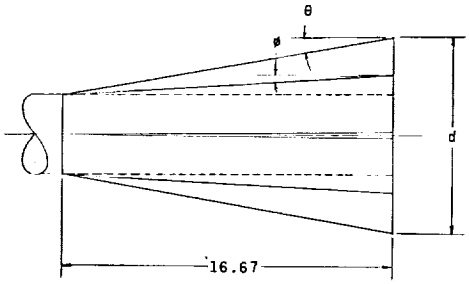

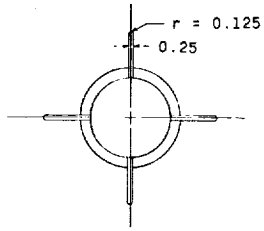

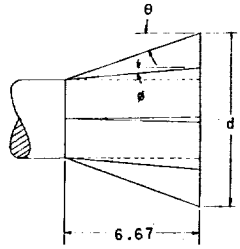

Long fin-flare configurations

θ,deg	d_{fin}	ø,deg	d_{flare}
5.0	6.92	0.0	4.00
"	"	2.5	5.46
"	"	5.0	6.92
7.5	8.39	0.0	4.00
"	"	2.5	5.46
"	"	5.0	6.92
"	"	7.5	8.39
10.0	9.80	0.0	4.00
"	"	2.5	5.46
"	"	5.0	6.92
"	"	10.0	9.80
12.1	11.02	0.0	4.00
"	"	5.0	6.92
"	"	10.0	9.80
"	"	12.1	11.02

Short fin-flare configurations

θ,deg	d_{fin}	ø,deg	d_{flare}
10.0	6.350	0.0	4.000
"	"	5.0	5.170
"	"	10.0	6.350
19.3	8.670	0.0	4.000
"	"	5.0	5.170
"	"	10.0	6.350
"	"	19.3	8.670
27.8	11.020	0.0	4.000
"	"	10.0	6.350
"	"	19.3	8.670
"	"	27.8	11.020

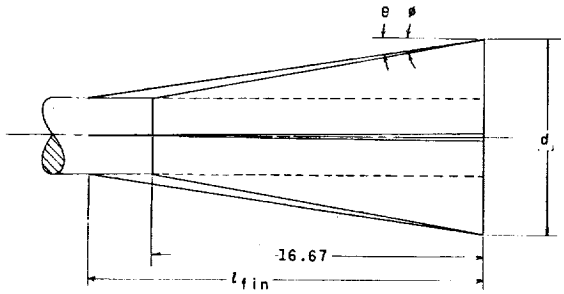

Long flare with fin of low aspect ratio

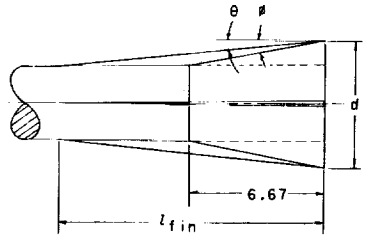

Short flare with fin of low aspect ratio

θ,deg	l_{fin}	d	ø,deg	Basic fin having equal area θ,deg	Basic fin having equal area d_{fin}
8.32	19.817	9.800	10.0	12.1	11.020

θ,deg	l_{fin}	d	ø,deg	Basic fin having equal area θ,deg	Basic fin having equal area d_{fin}
1.28	26.614	5.170	5.0	19.3	8.670
5.03	13.250	6.350	10.0	19.3	8.670
13.15	10.007	8.670	19.3	27.8	11.020

Figure 1.- Drawing of model. All dimensions are in inches unless otherwise indicated.

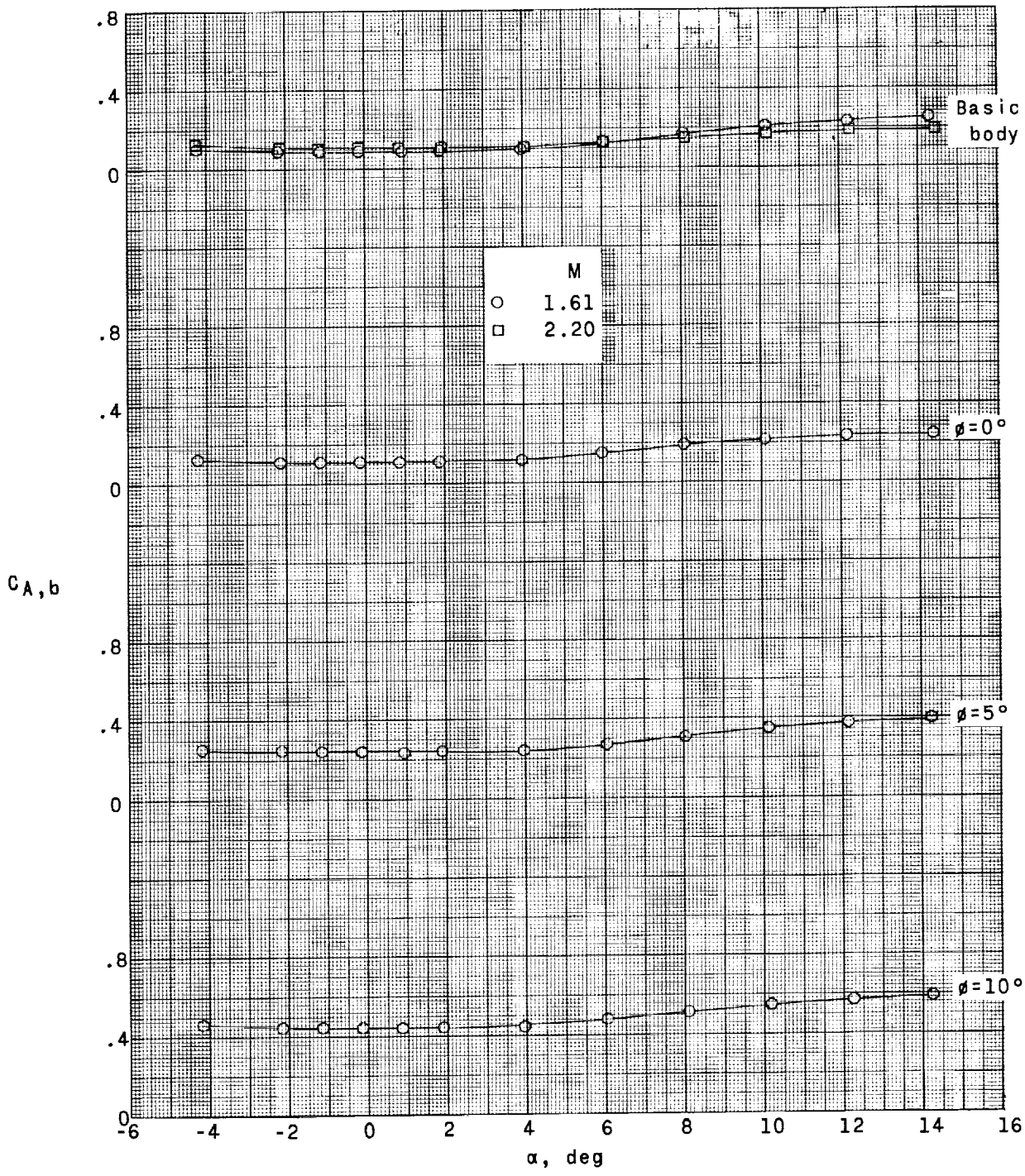

(a) Short fin-flare configurations. $\theta = 10^{\circ}$.

Figure 2.- Variation of base axial-force coefficient $C_{A,b}$ with angle of attack.

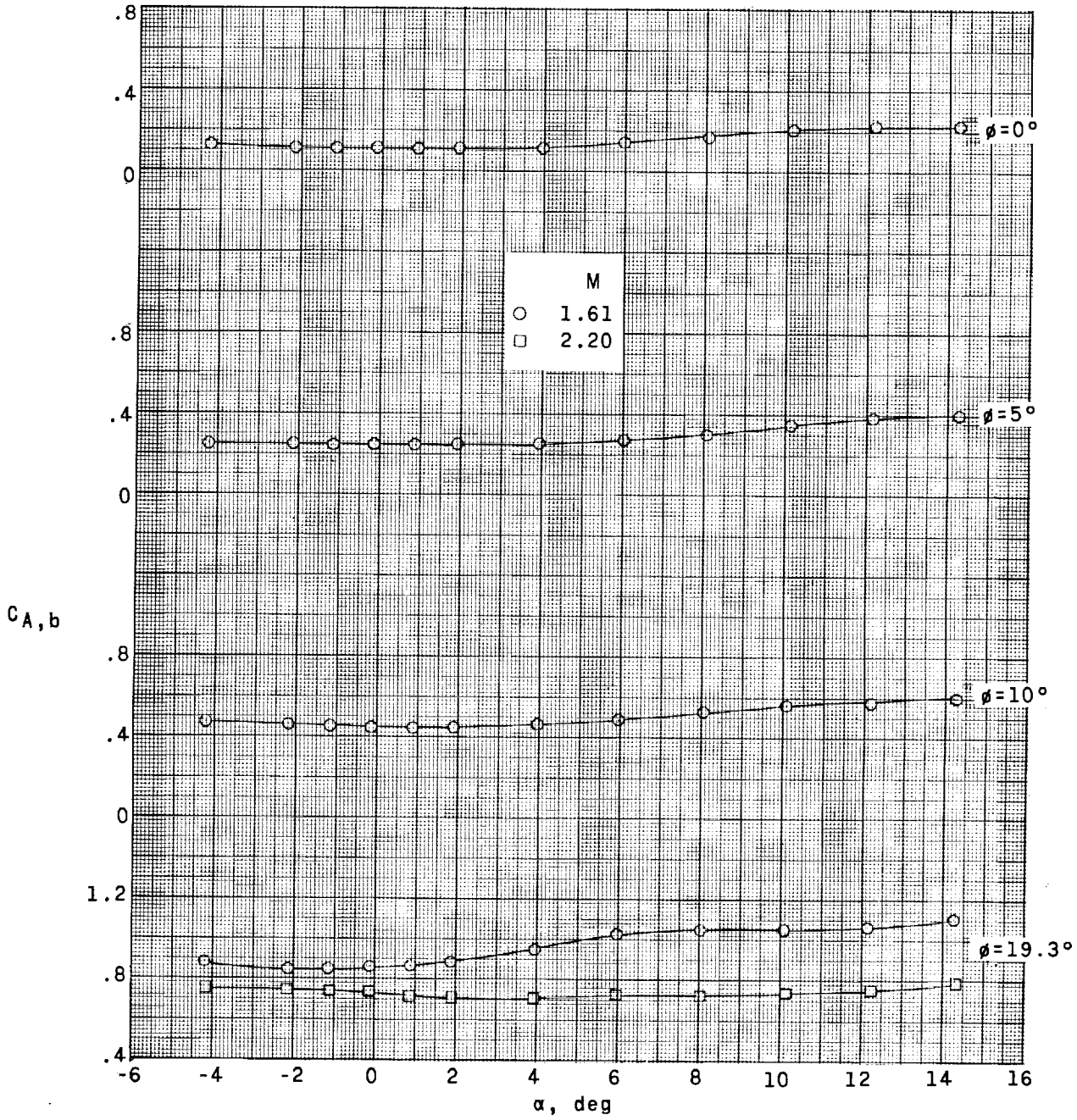

(b) Short fin-flare configurations. $\theta = 19.3°$.

Figure 2.- Continued.

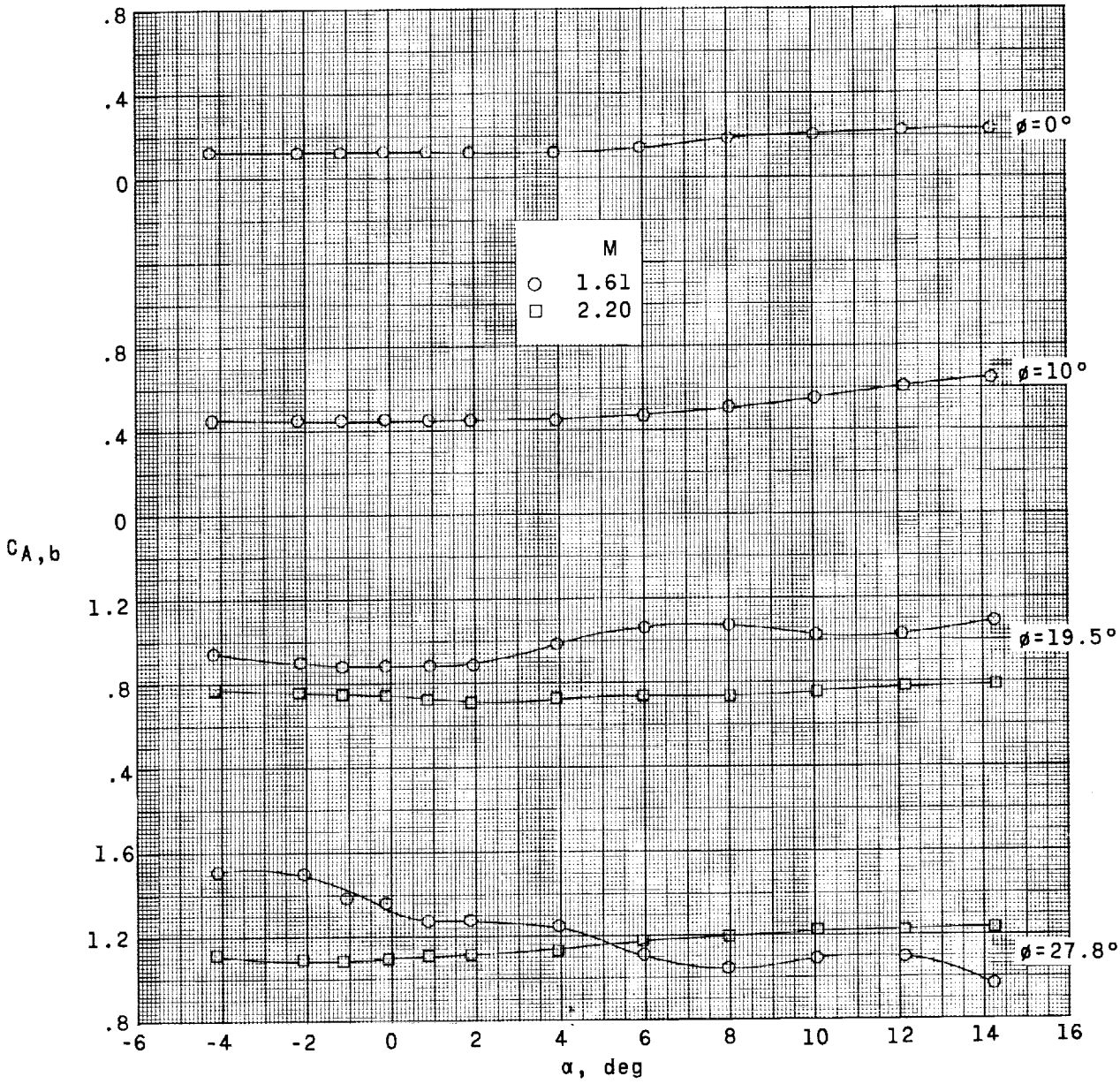

(c) Short fin-flare configurations. $\theta = 27.8^{\circ}$.

Figure 2.- Continued.

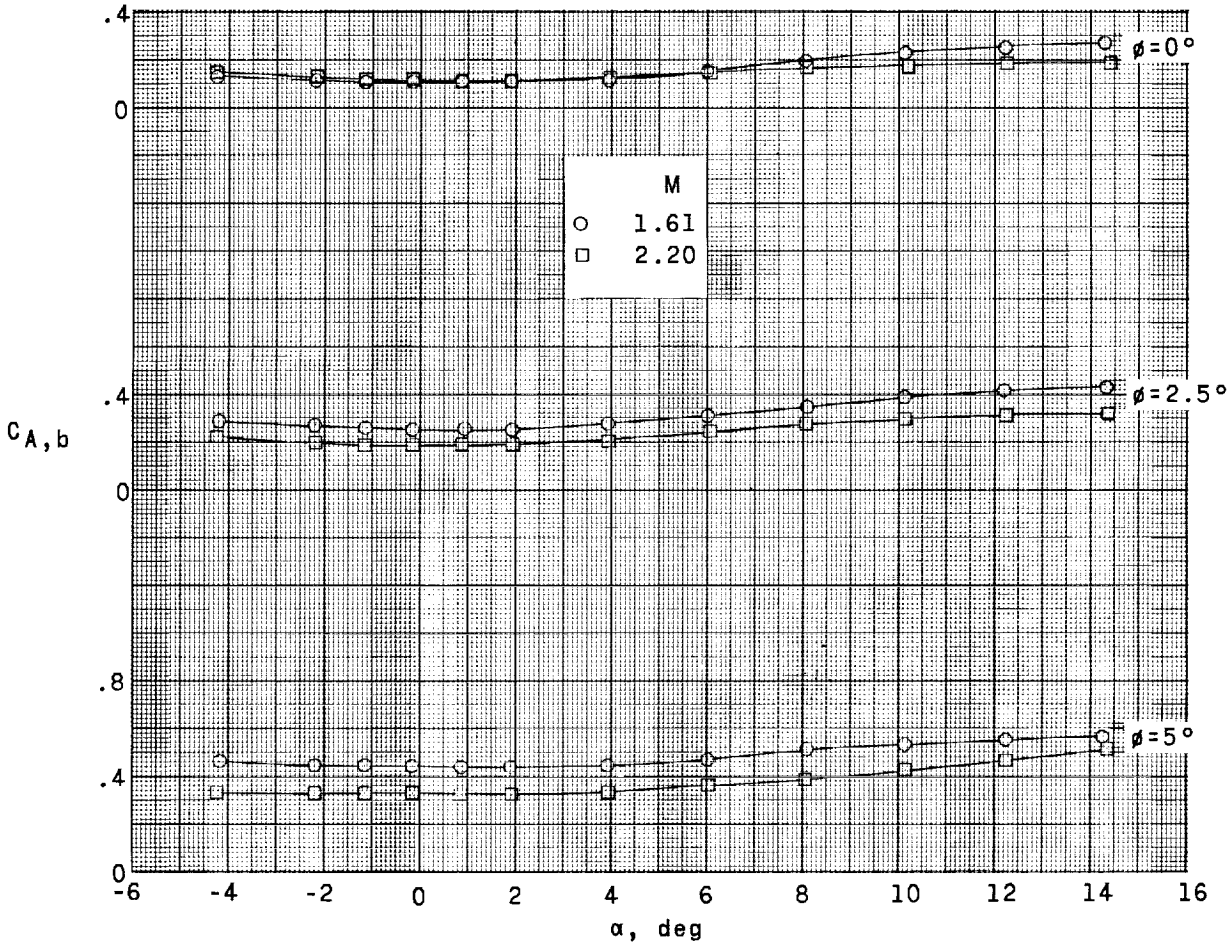

(d) Long fin-flare configurations. $\theta = 5^{\circ}$.

Figure 2.- Continued.

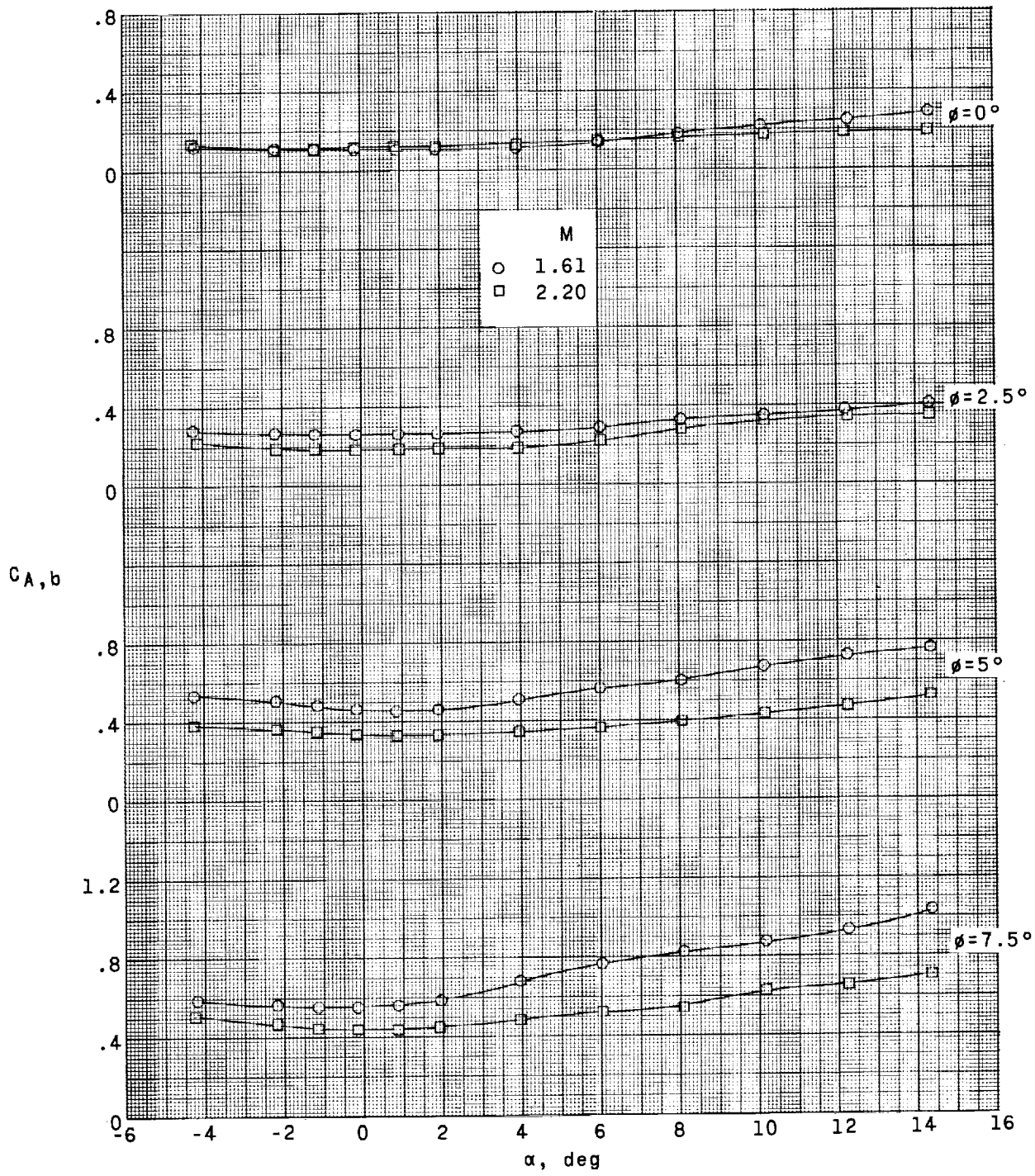

(e) Long fin-flare configurations. $\theta = 7.5^{\circ}$.

Figure 2.- Continued.

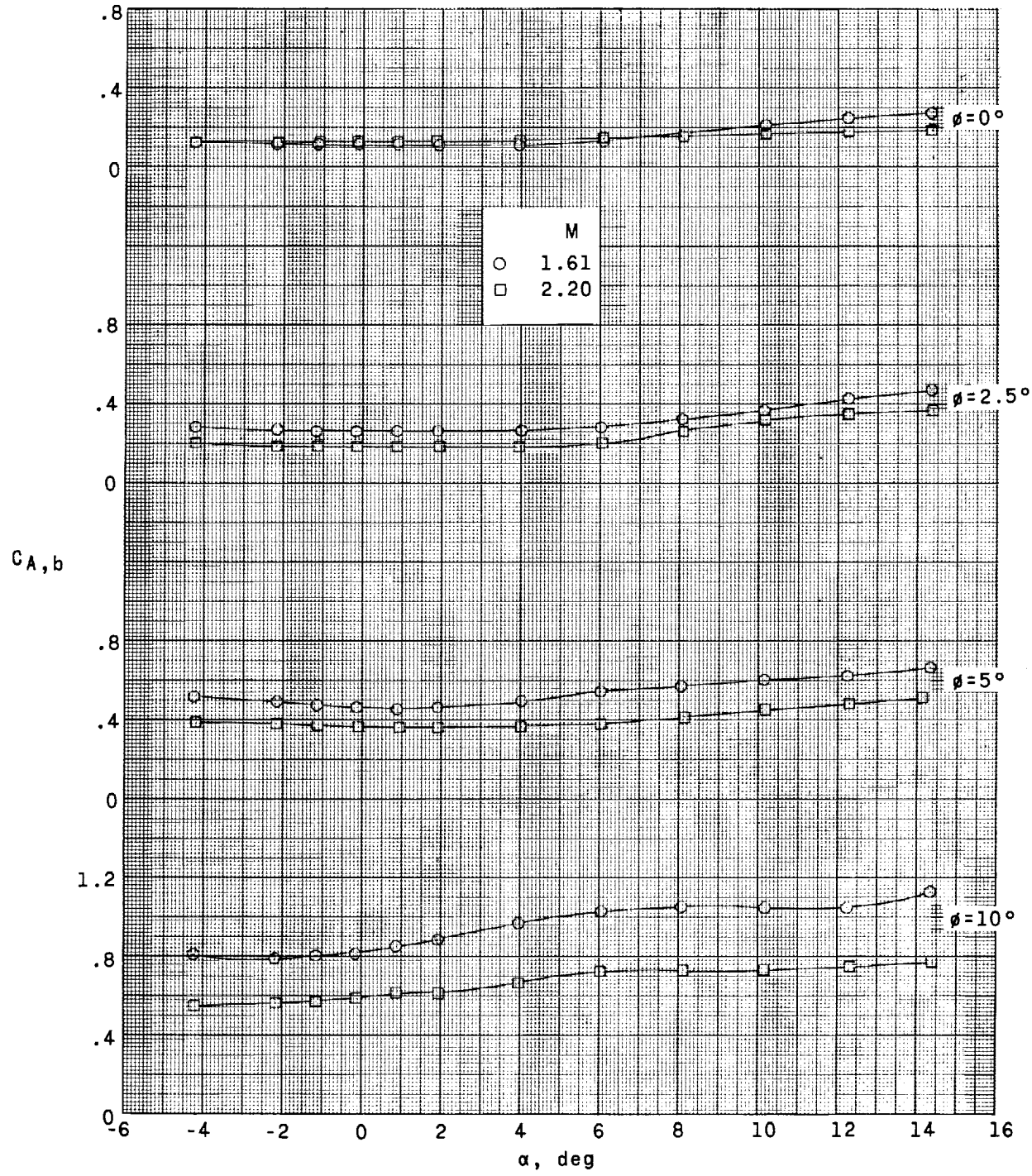

(f) Long fin-flare configurations. $\theta = 10^{o}$.

Figure 2.- Continued.

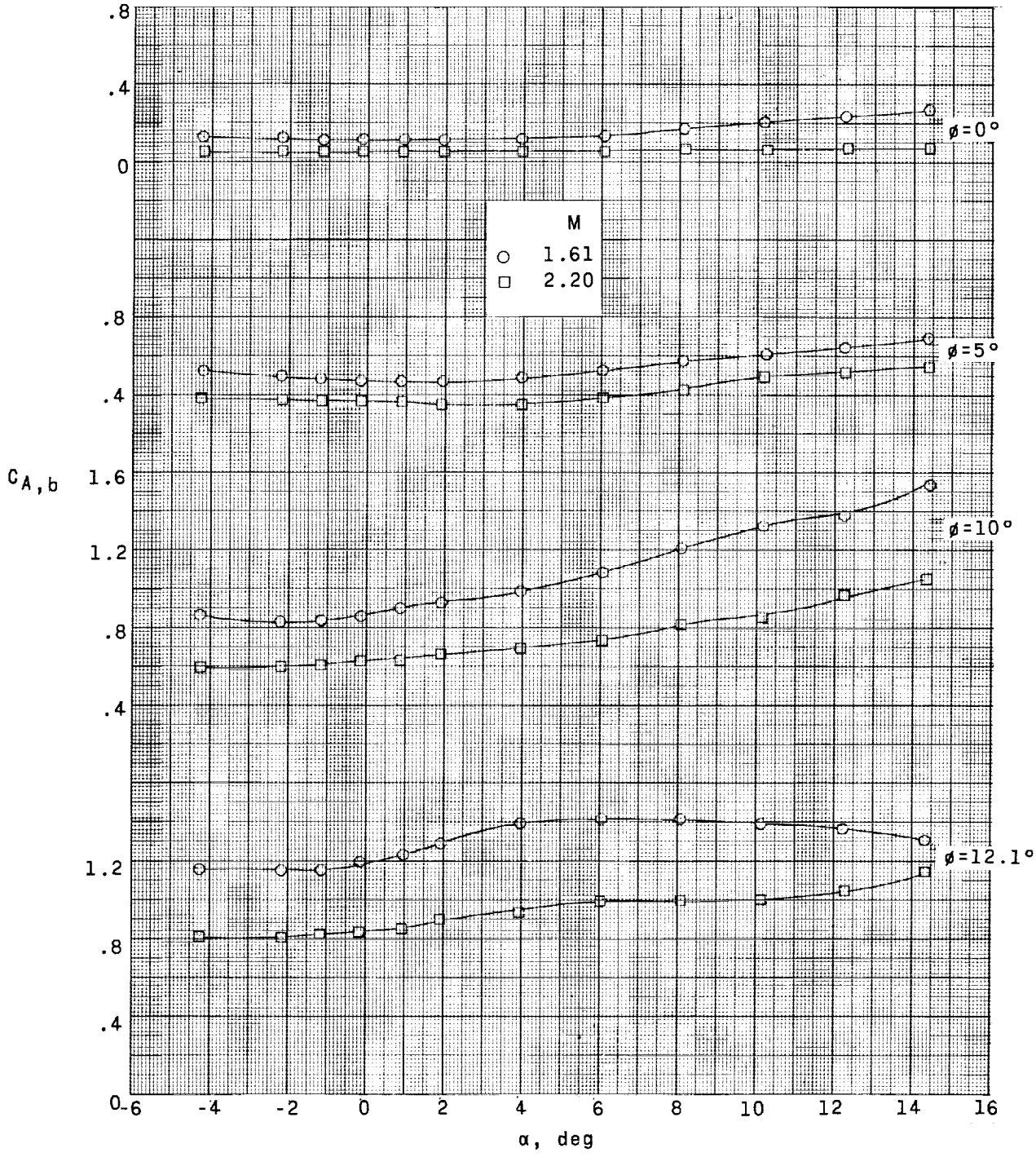

(g) Long fin-flare configurations. $\theta = 12.1^{\circ}$.

Figure 2.- Continued.

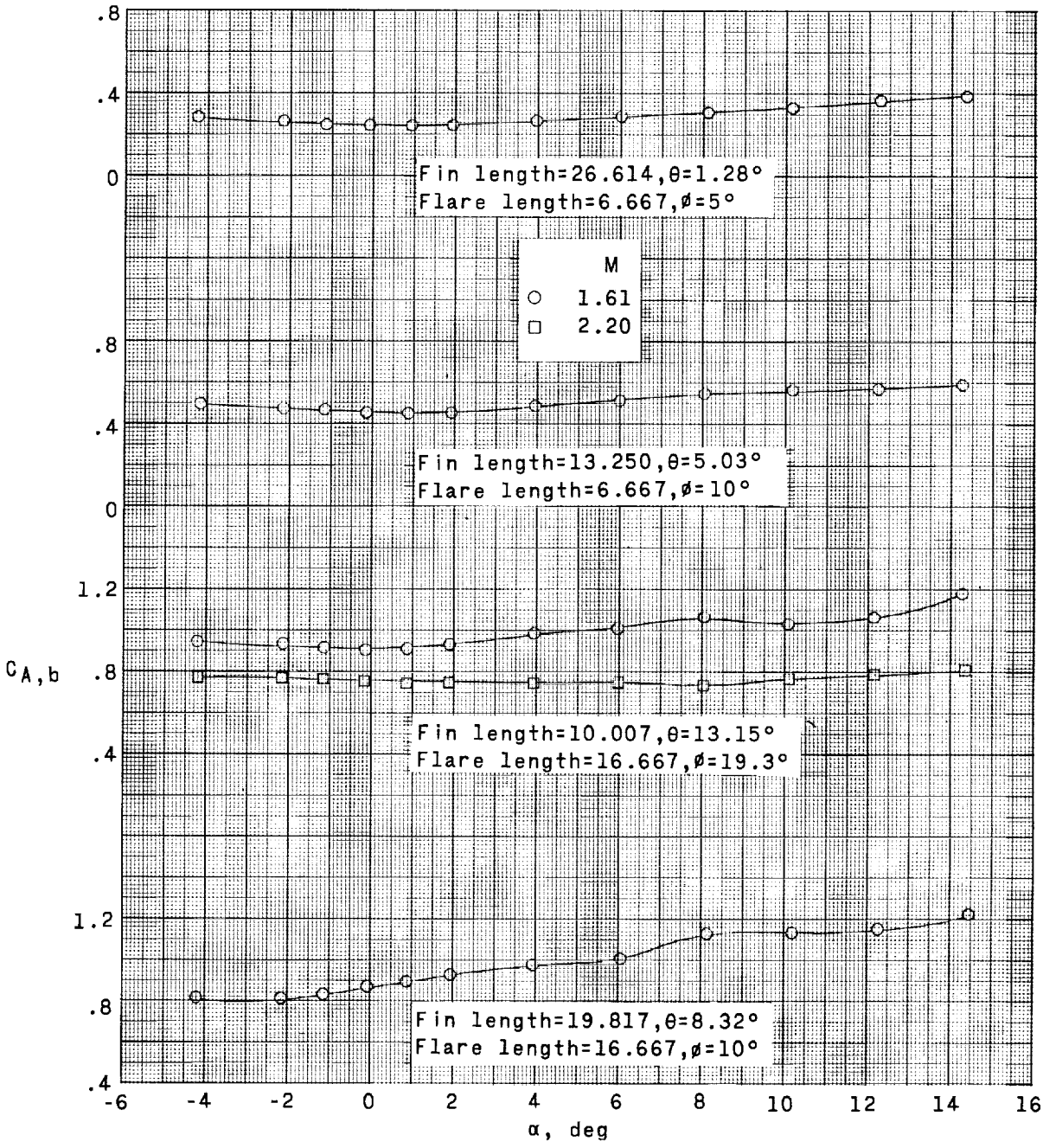

(h) Fin-flare configurations with fins of low aspect ratio.

Figure 2.- Concluded.

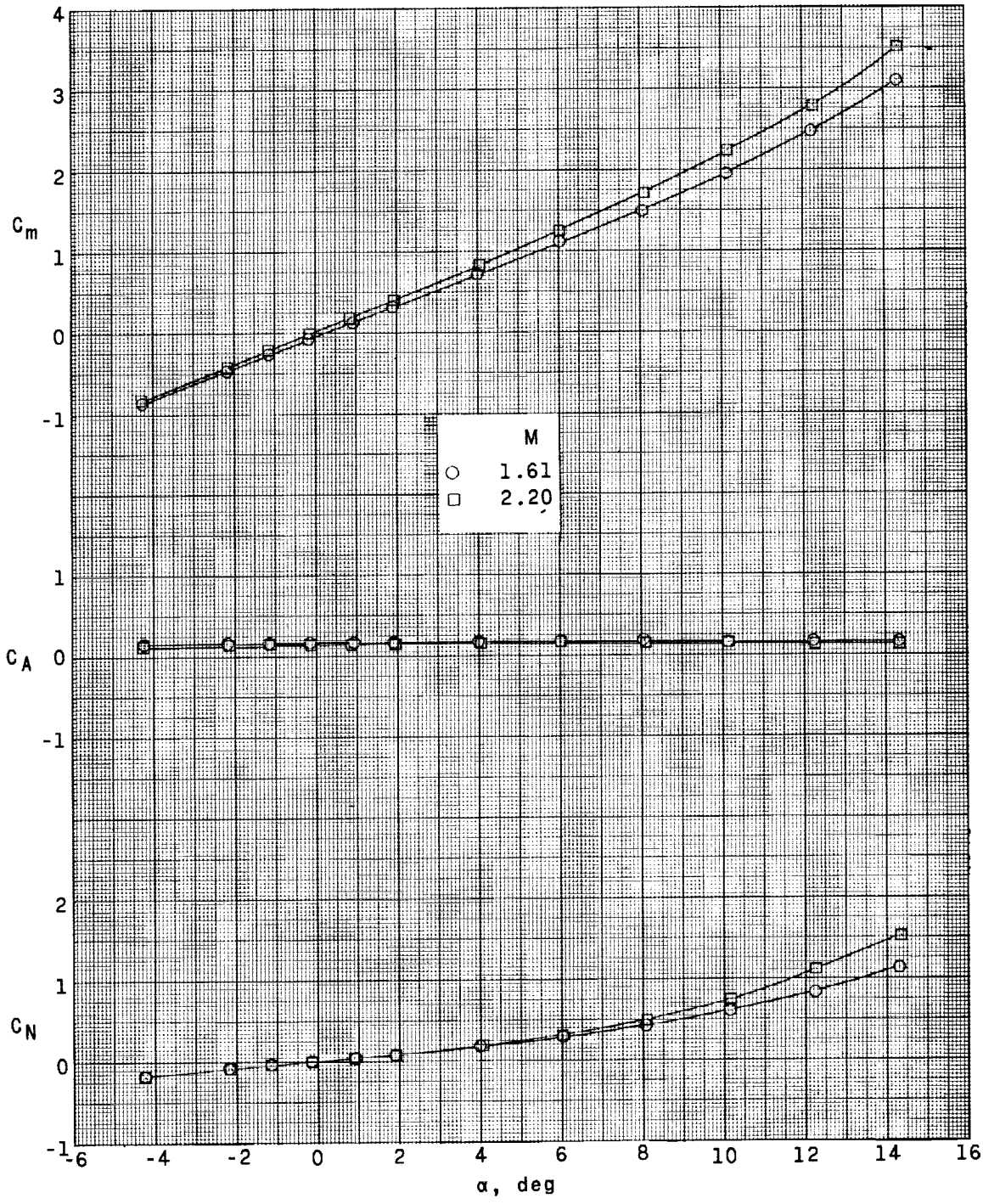

Figure 3.- Aerodynamic characteristics of basic body.

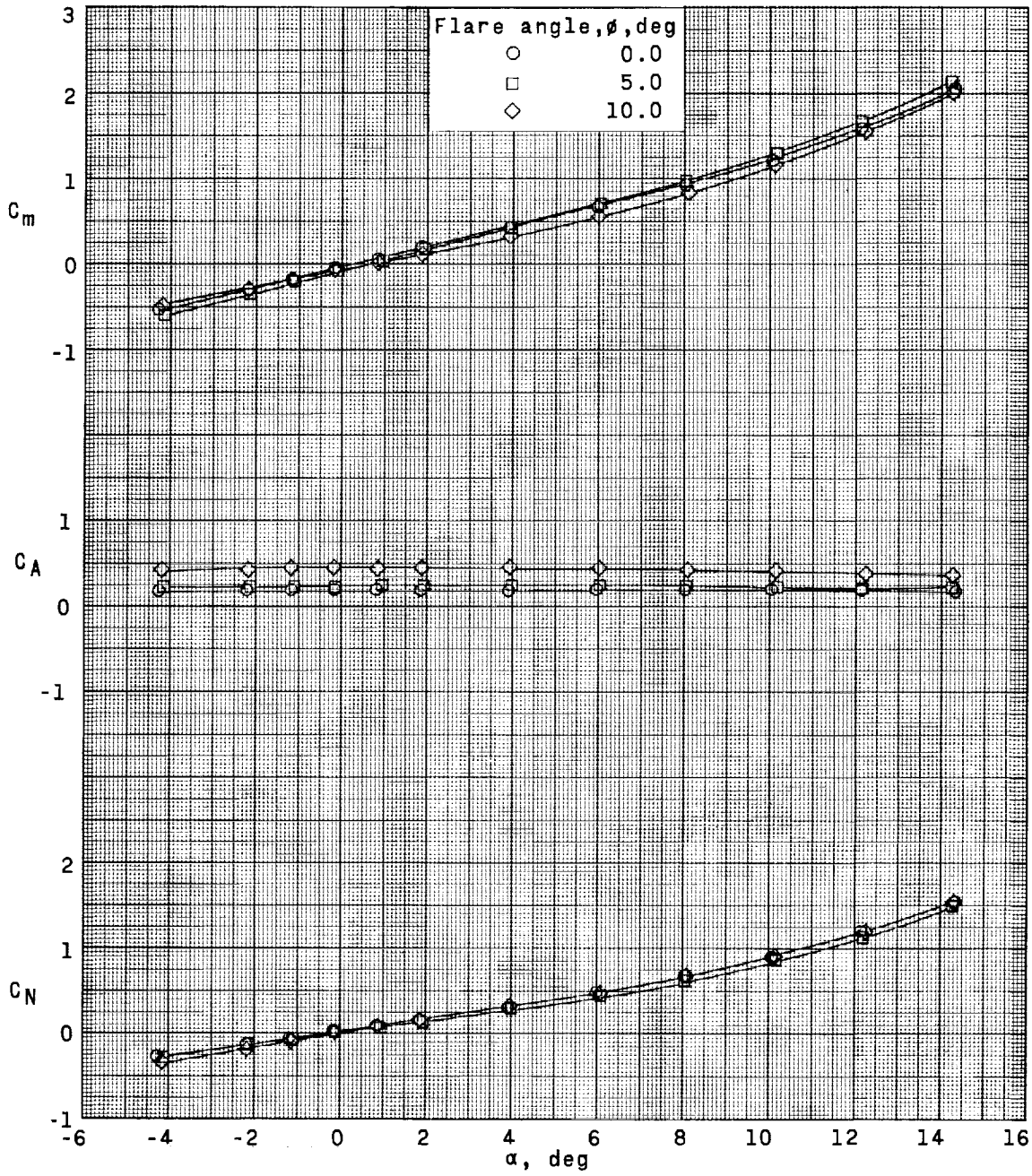

(a) Short fin-flare configurations. $\theta = 10^{\circ}$; M = 1.61.

Figure 4.- Aerodynamic characteristics of basic fin-flare combinations.

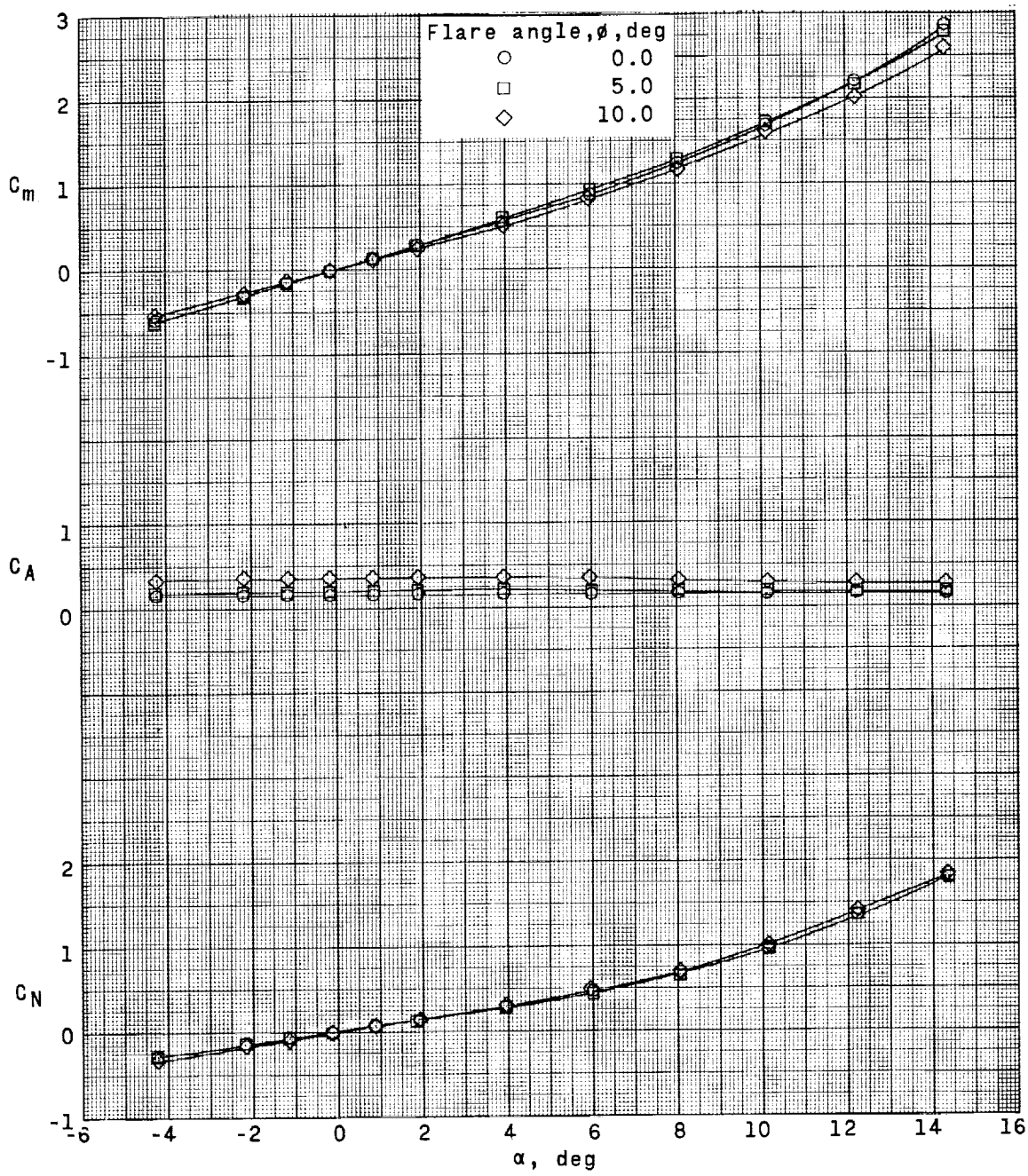

(b) Short fin-flare configurations. $\theta = 10^{o}$; M = 2.20.

Figure 4.- Continued.

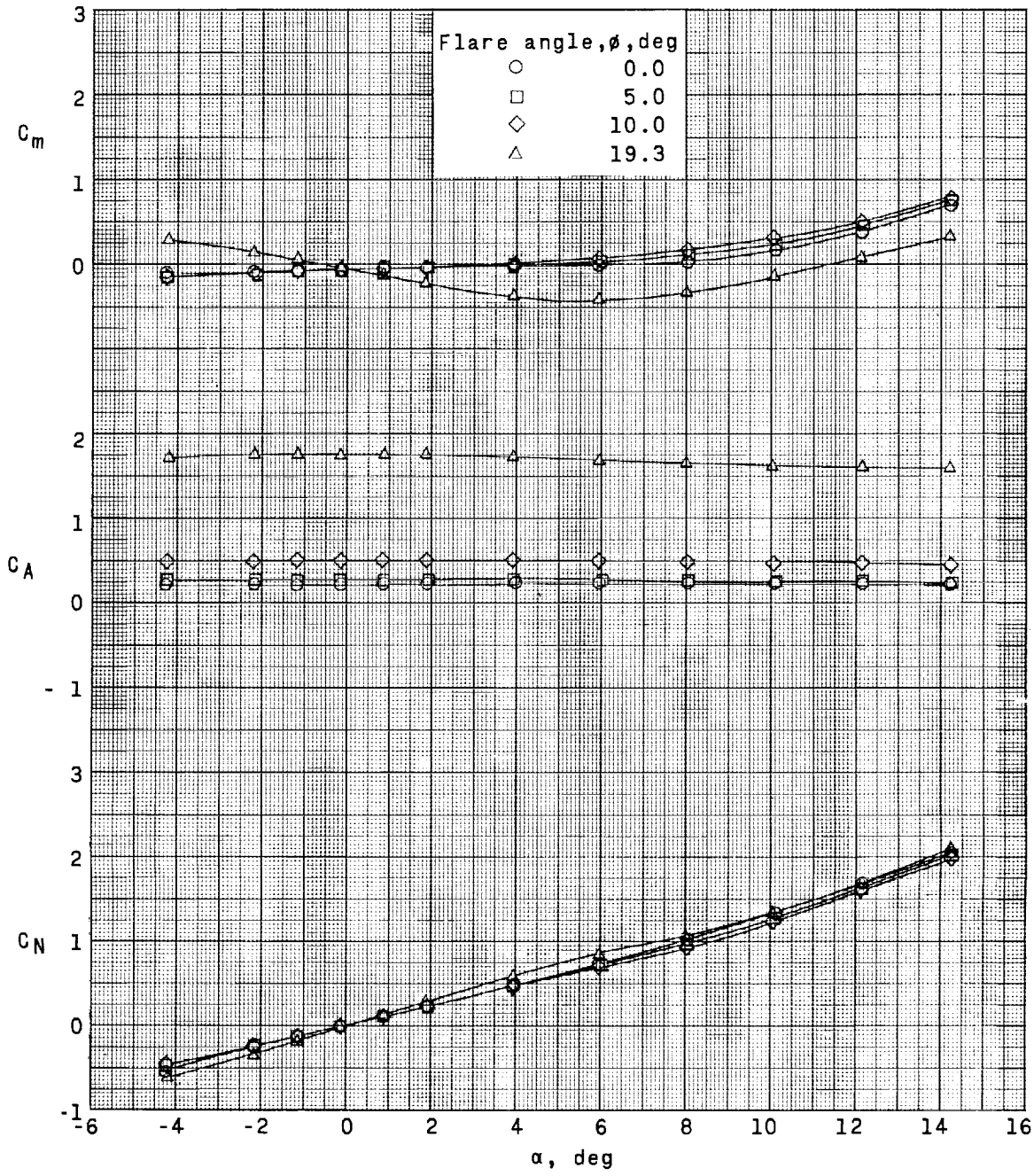

(c) Short fin-flare configurations. $\theta = 19.3^{o}$; M = 1.61.

Figure 4.- Continued.

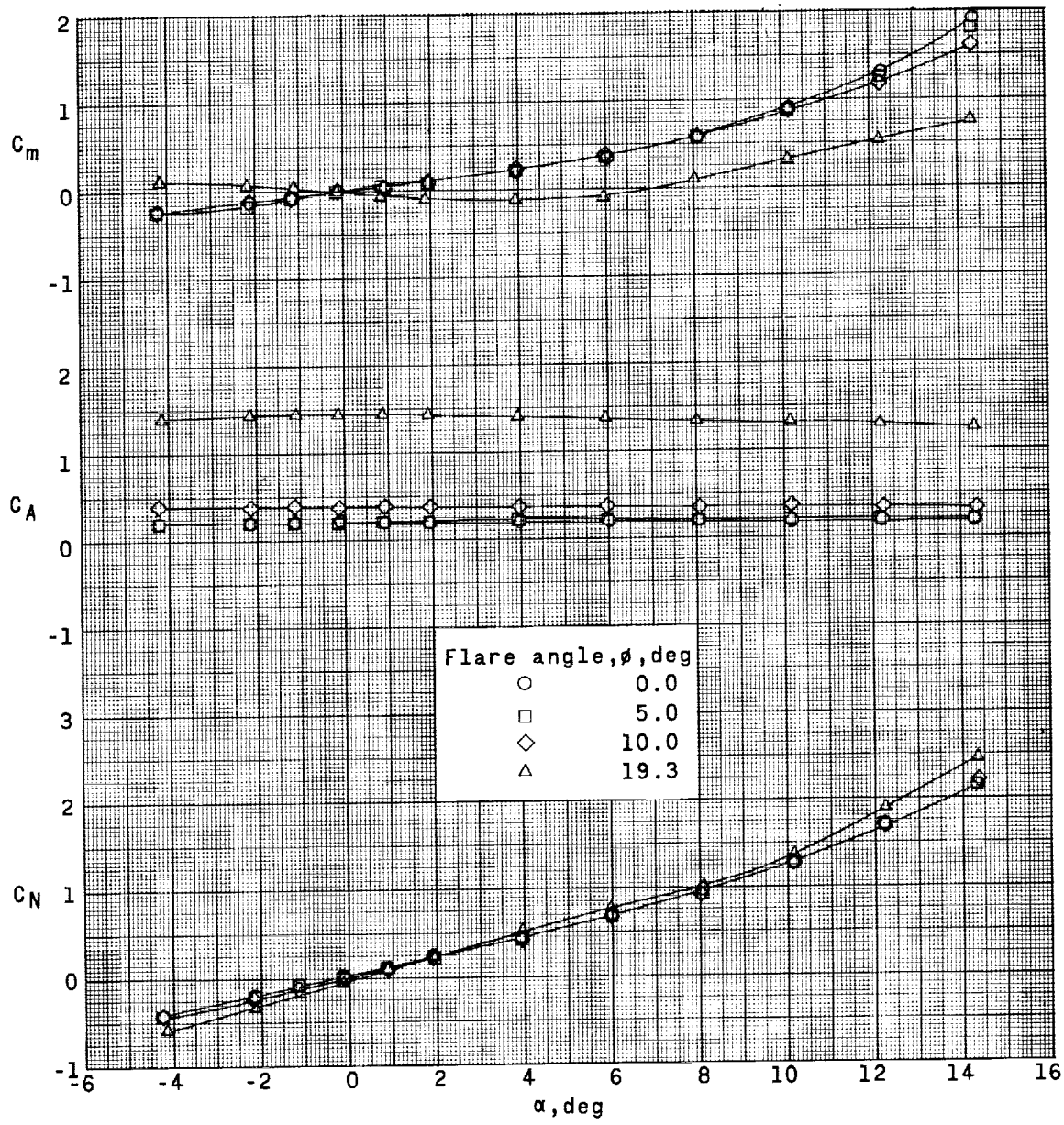

(d) Short fin-flare configurations. θ = 19.3°; M = 2.20.

Figure 4.- Continued.

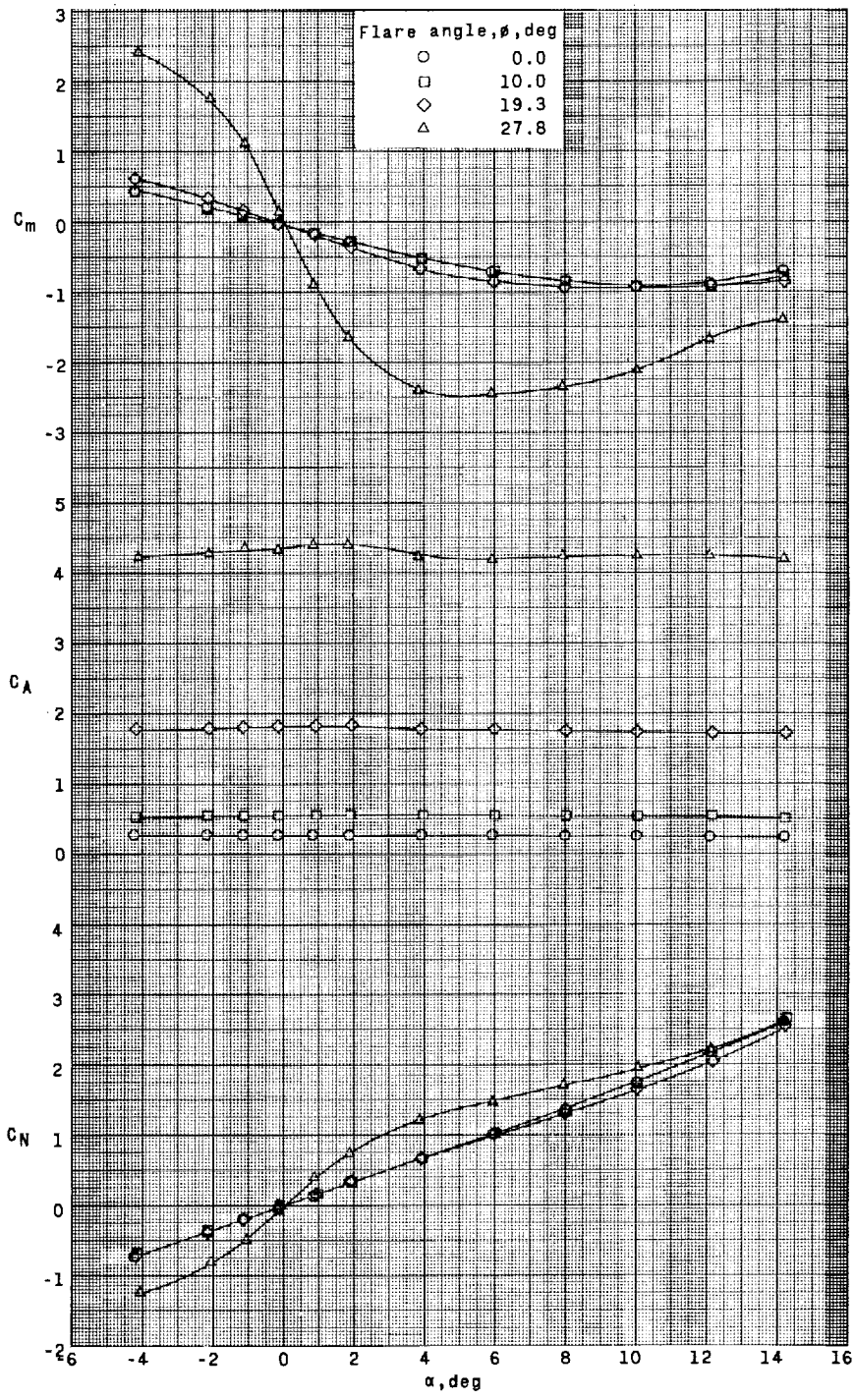

(e) Short fin-flare configurations. $\theta = 27.8^{\circ}$; M = 1.61.

Figure 4.- Continued.

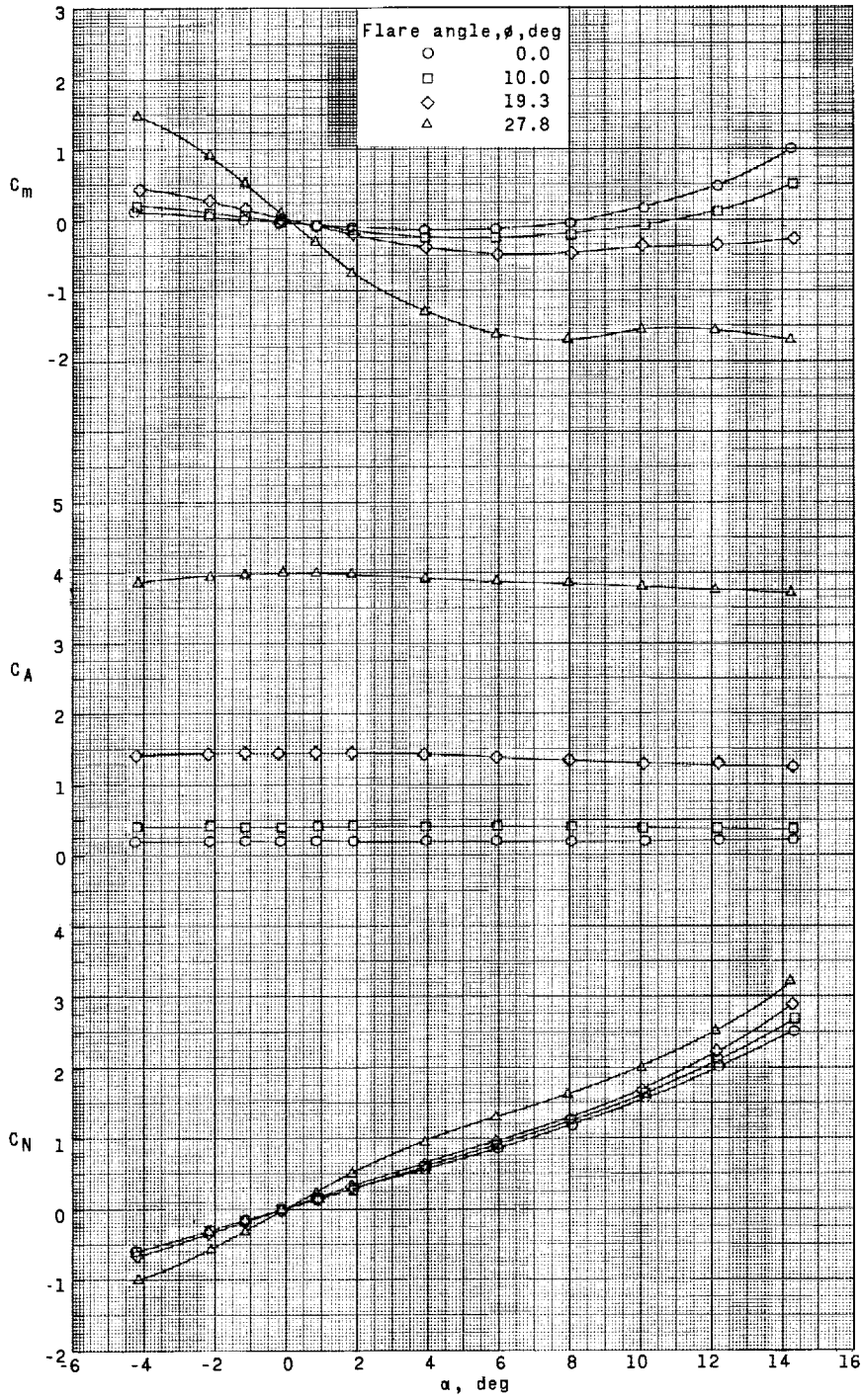

(f) Short fin-flare configurations. $\theta = 27.8^{\circ}$; $M = 2.20$.

Figure 4.- Continued.

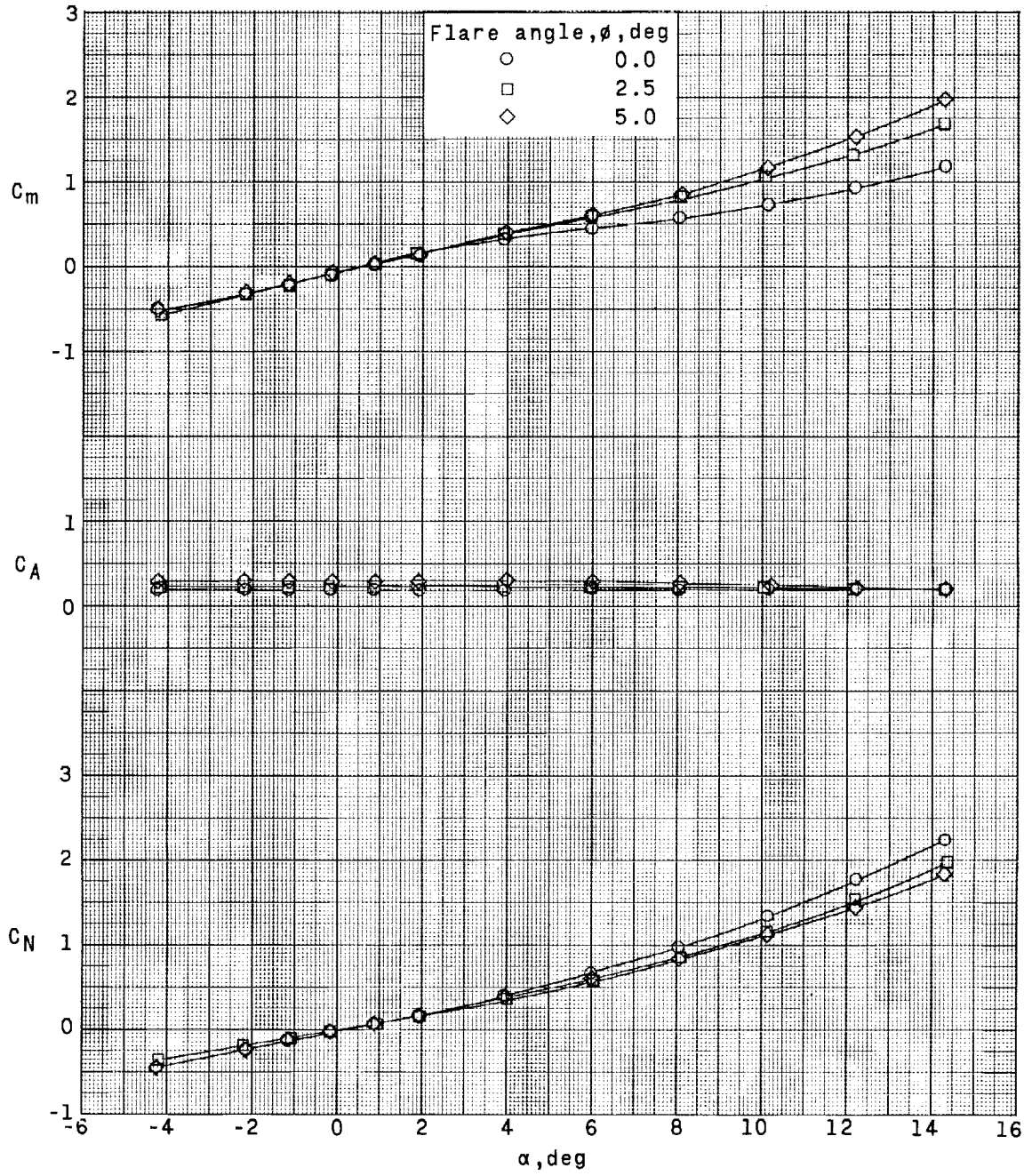

(g) Long fin-flare configurations. $\theta = 5^{\circ}$; M = 1.61.

Figure 4.- Continued.

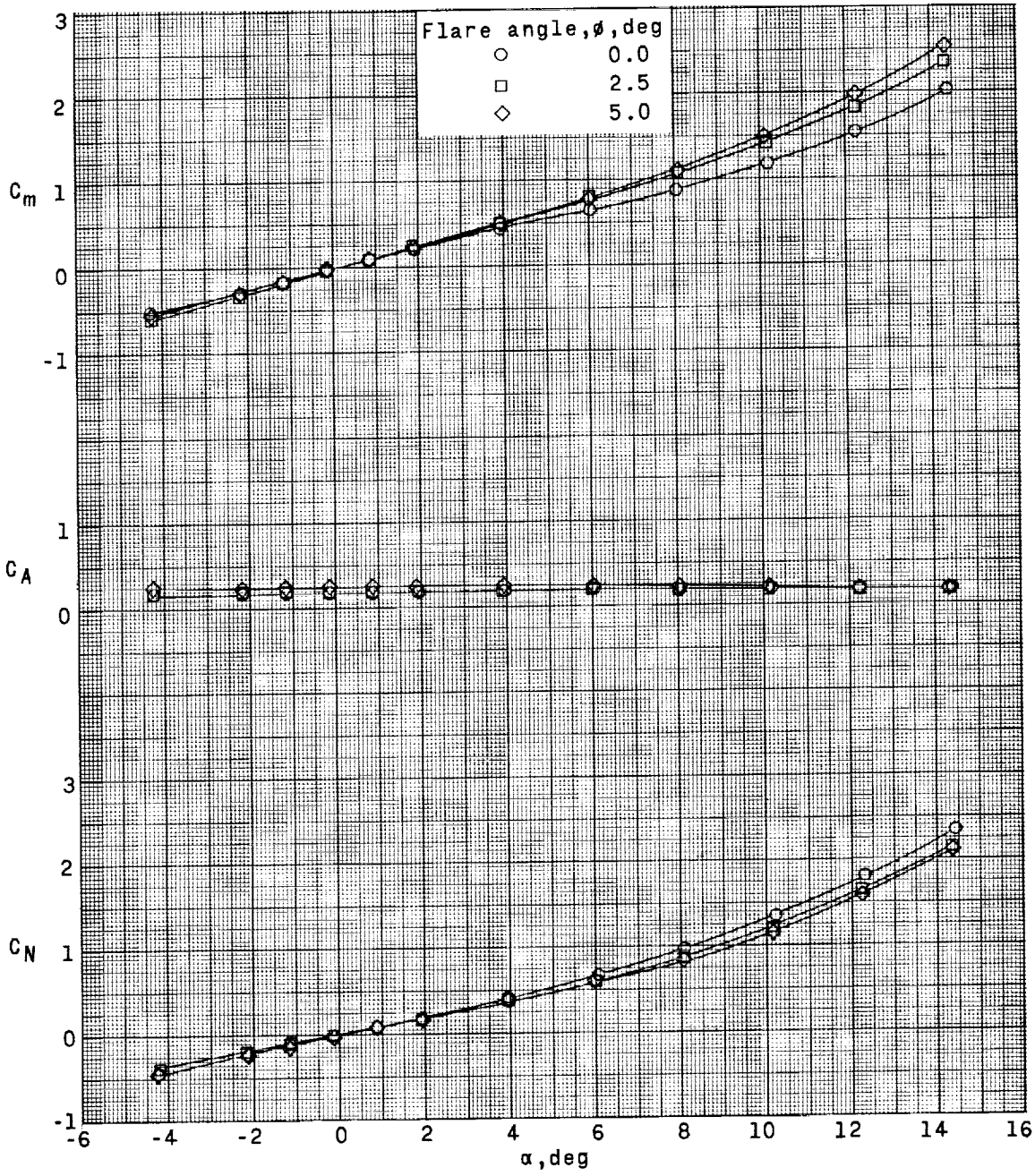

(h) Long fin-flare configurations. $\theta = 5^{\circ}$; $M = 2.20$.

Figure 4.- Continued.

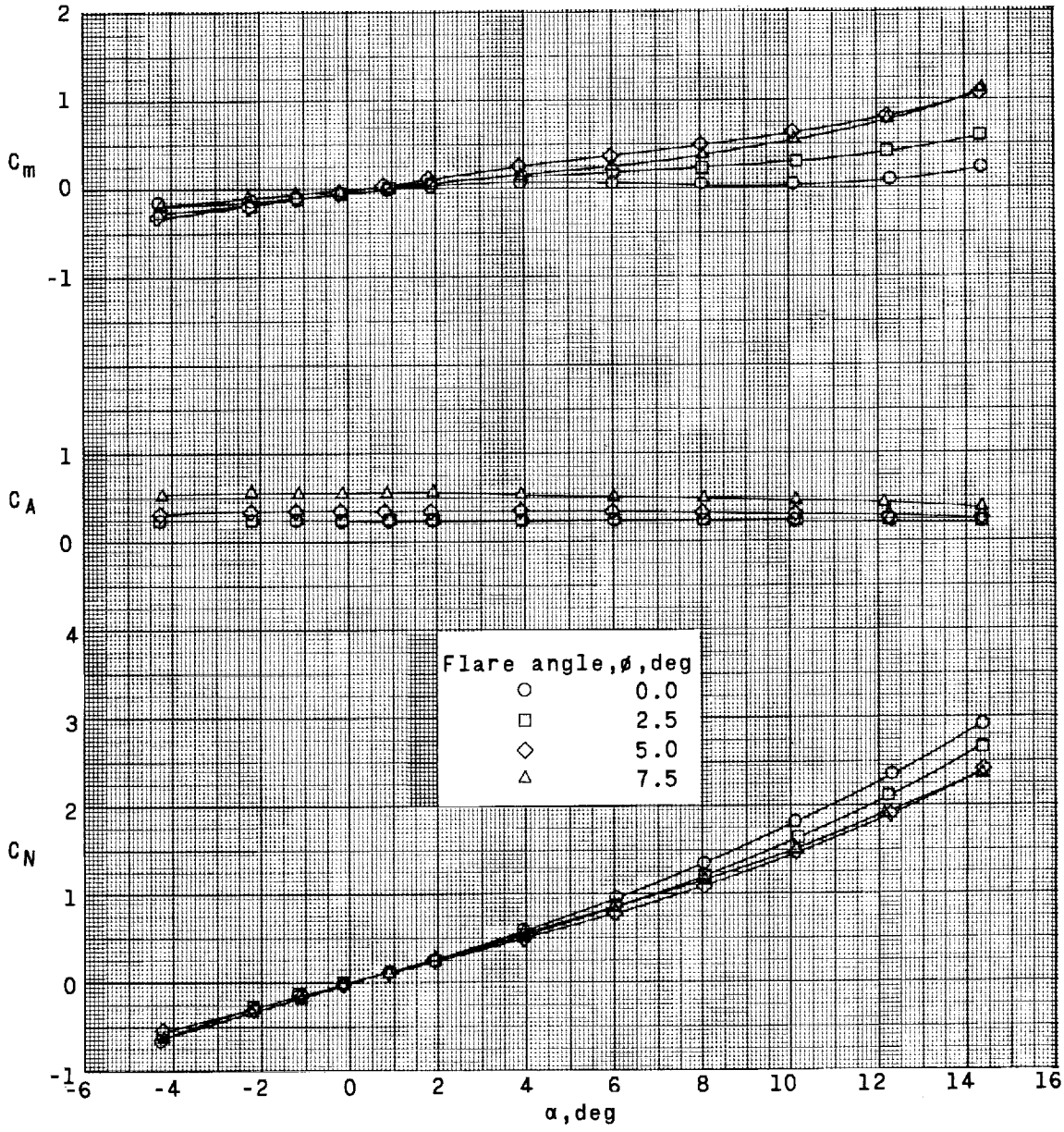

(i) Long fin-flare configurations. θ = 7.5°; M = 1.61.

Figure 4.- Continued.

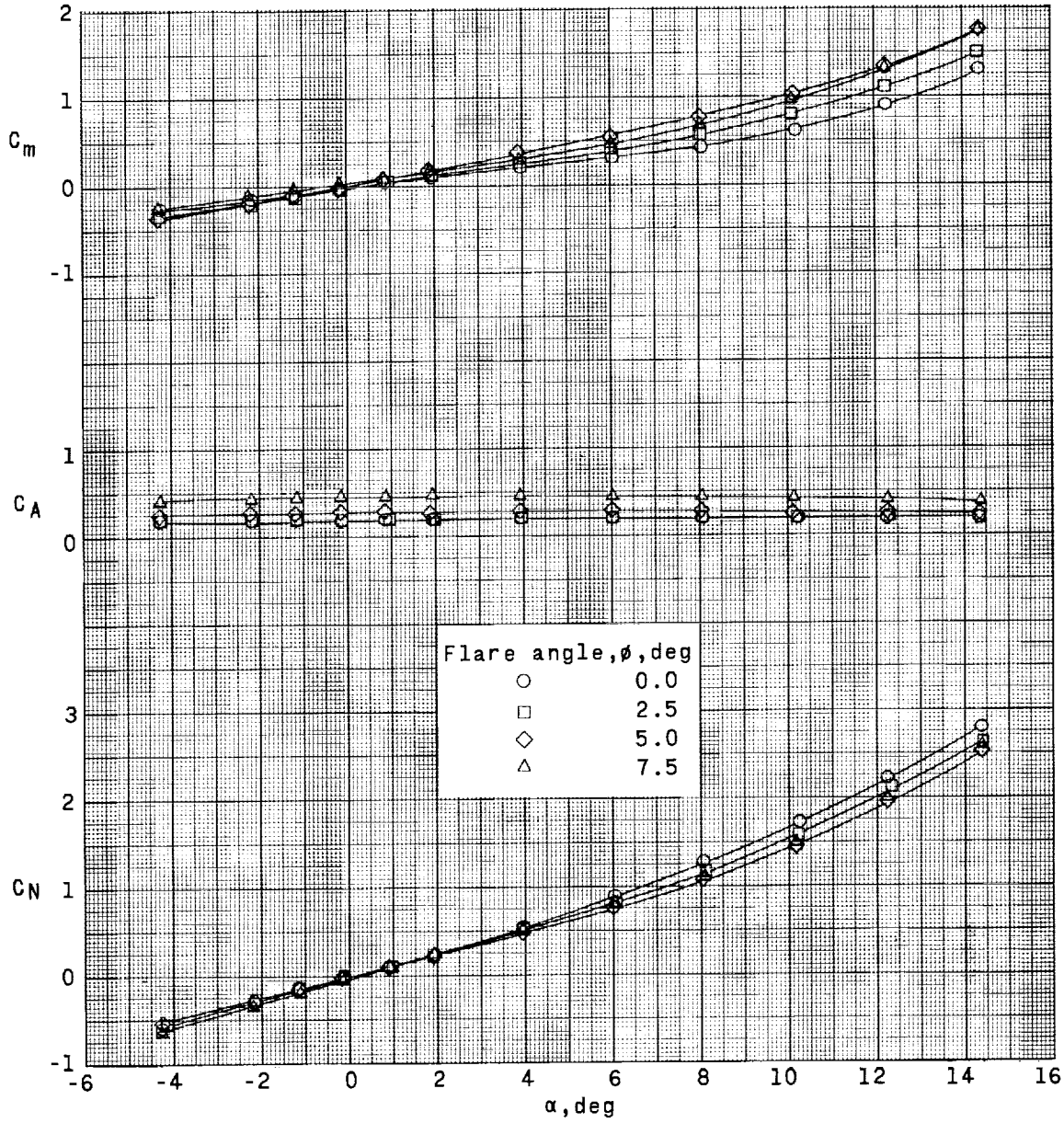

(j) Long fin-flare configurations. $\theta = 7.5^{\circ}$; M = 2.20.

Figure 4.- Continued.

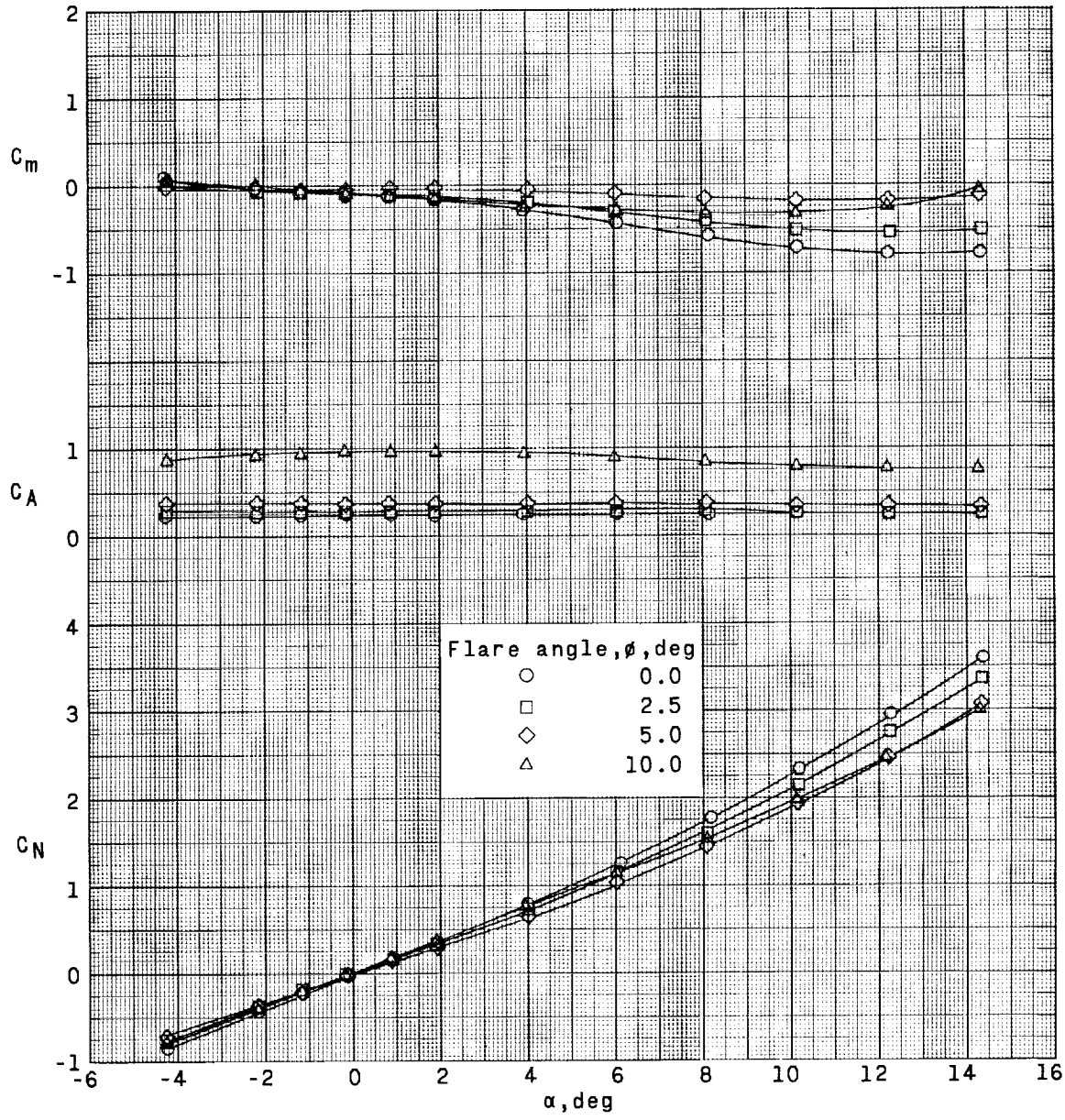

(k) Long fin-flare configurations. $\theta = 10^{\circ}$; M = 1.61.

Figure 4.- Continued.

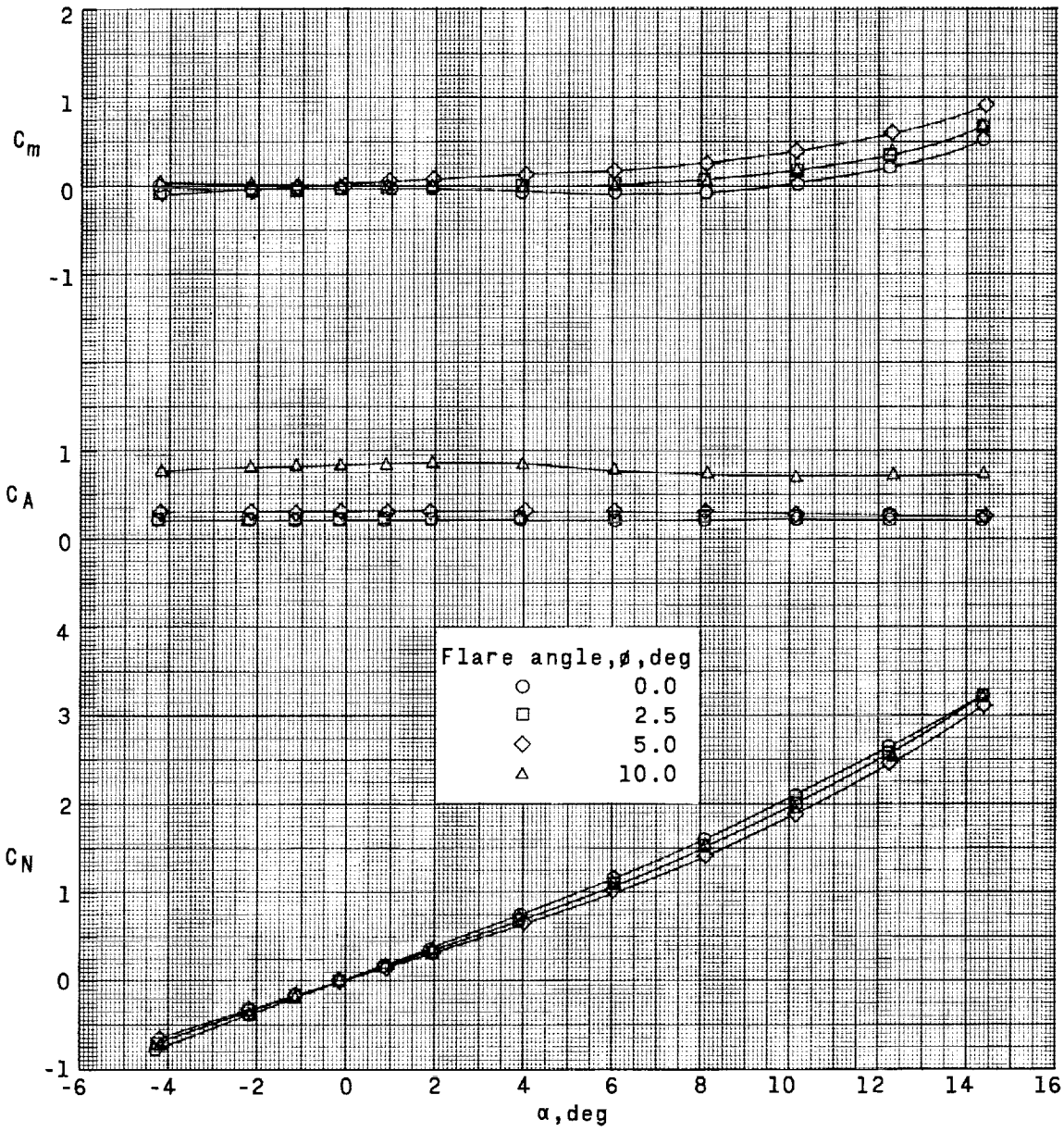

(l) Long fin-flare configurations. $\theta = 10^{o}$; M = 2.20.

Figure 4.- Continued.

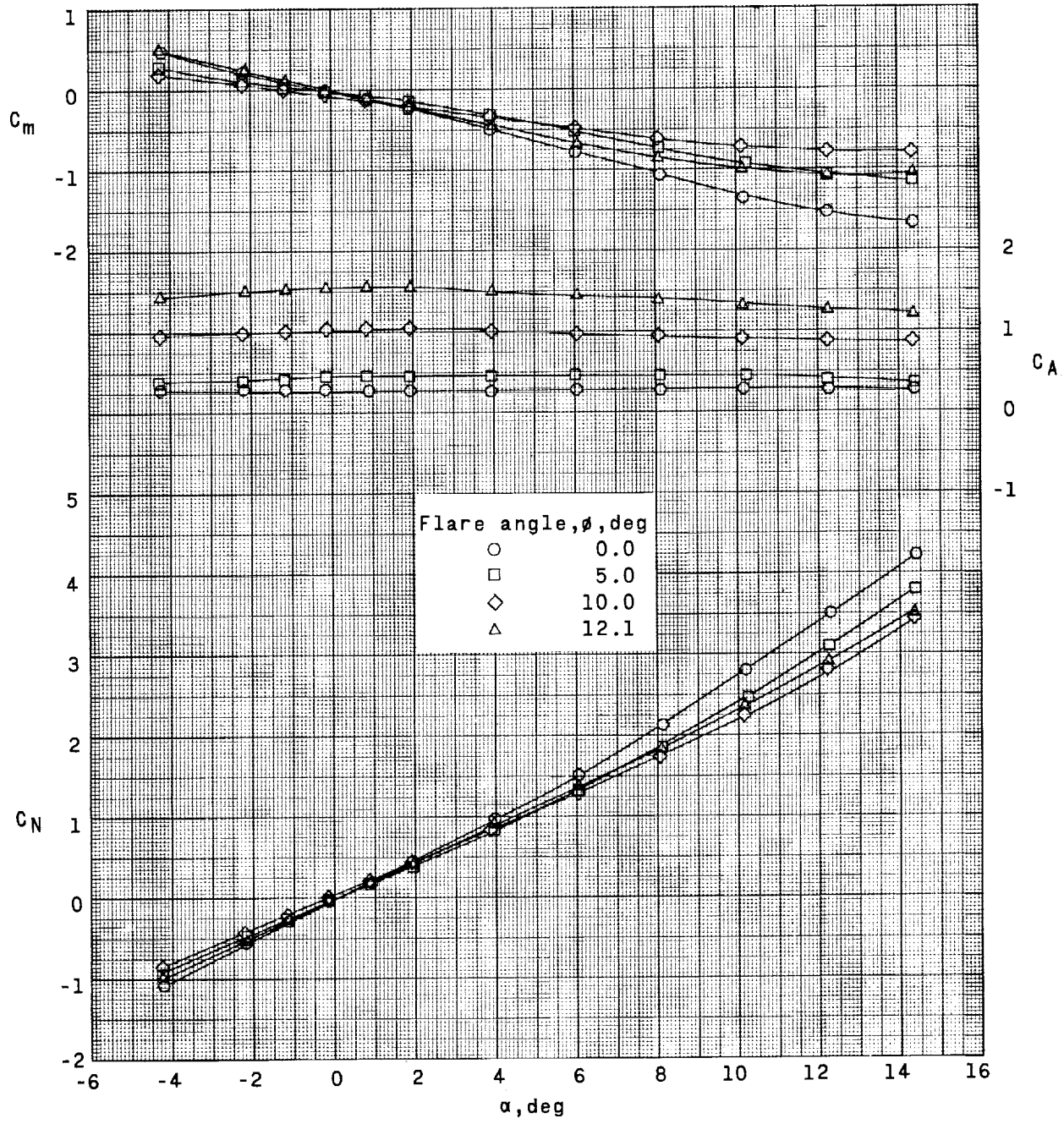

(m) Long fin-flare configurations. $\theta = 12.1^{\circ}$; M = 1.61.

Figure 4.- Continued.

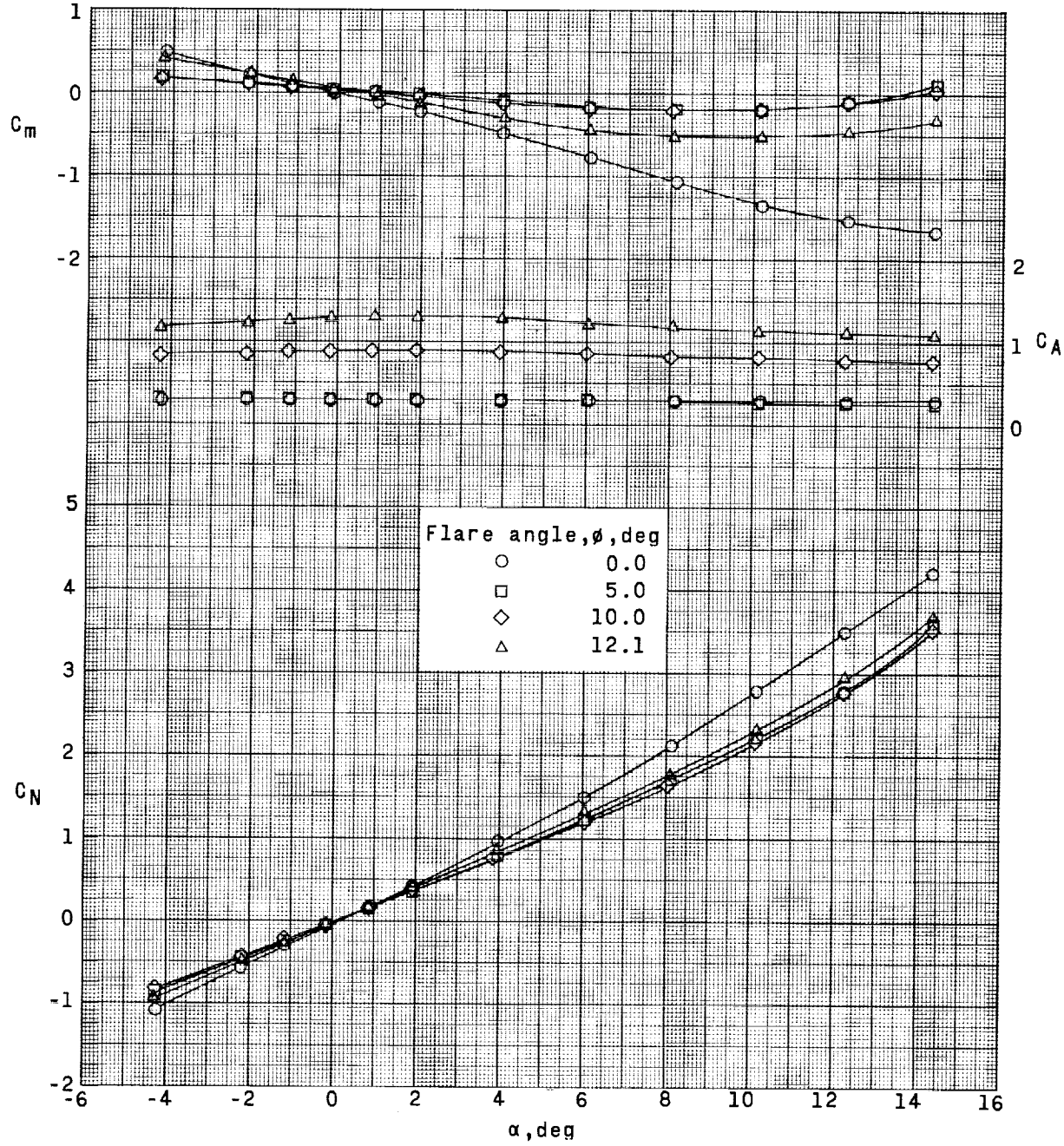

(n) Long fin-flare configurations. $\theta = 12.1^{\circ}$; M = 2.20.

Figure 4.- Concluded.

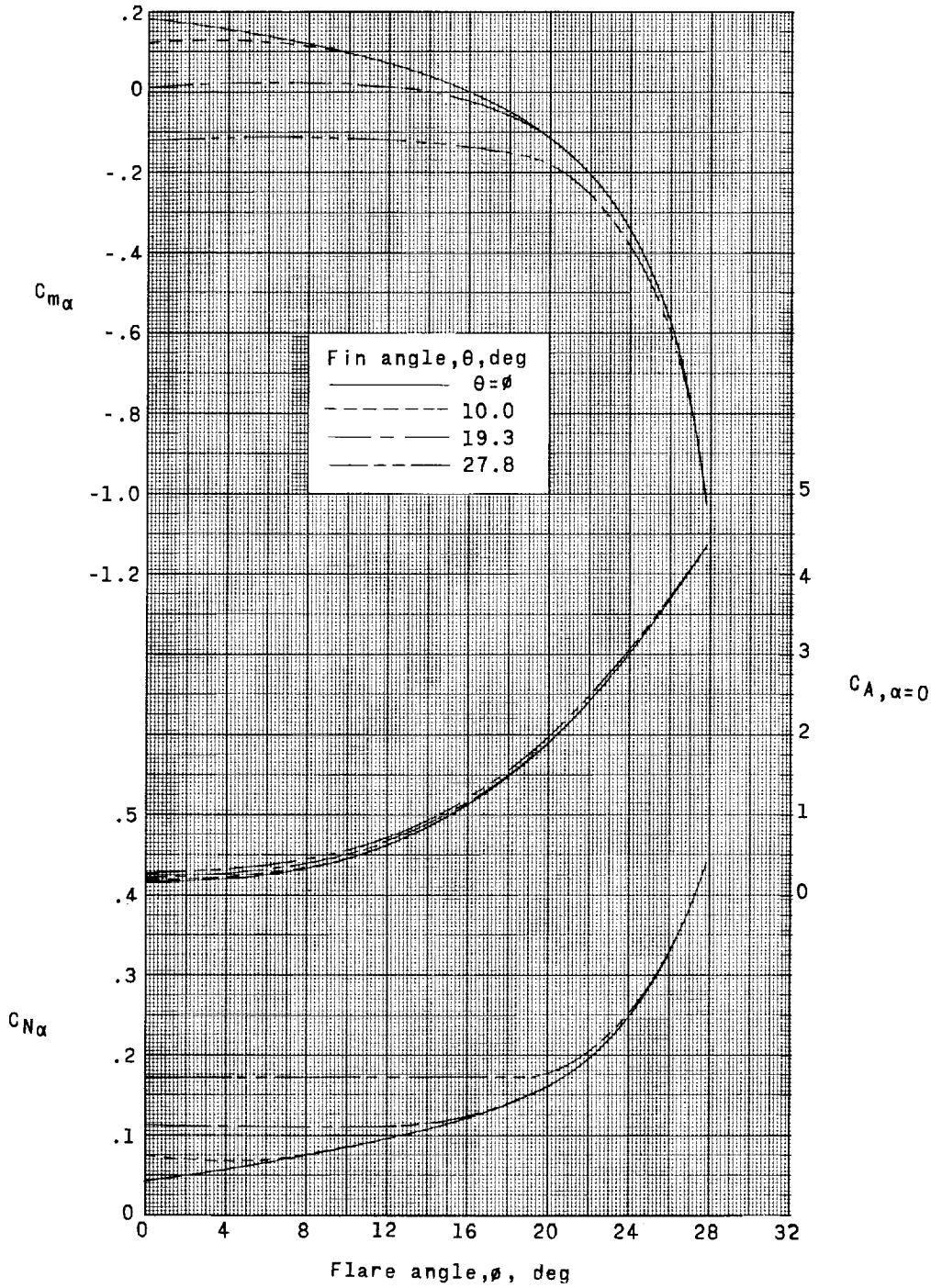

(a) Short fin-flare configurations. M = 1.61.

Figure 5.- Effect of combinations of fin angle and flare angle on static longitudinal stability.

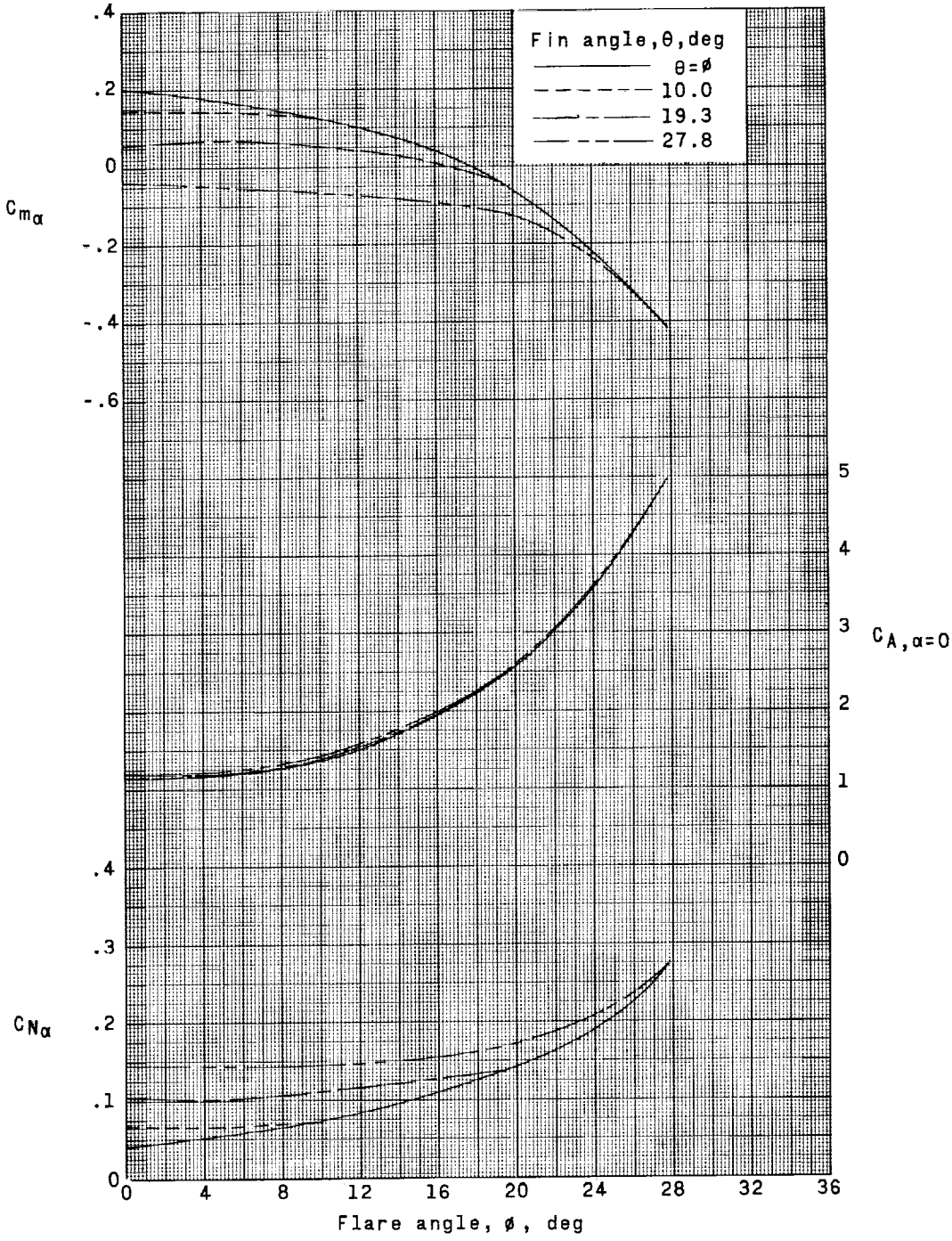

(b) Short fin-flare configurations. M = 2.20.

Figure 5.- Continued.

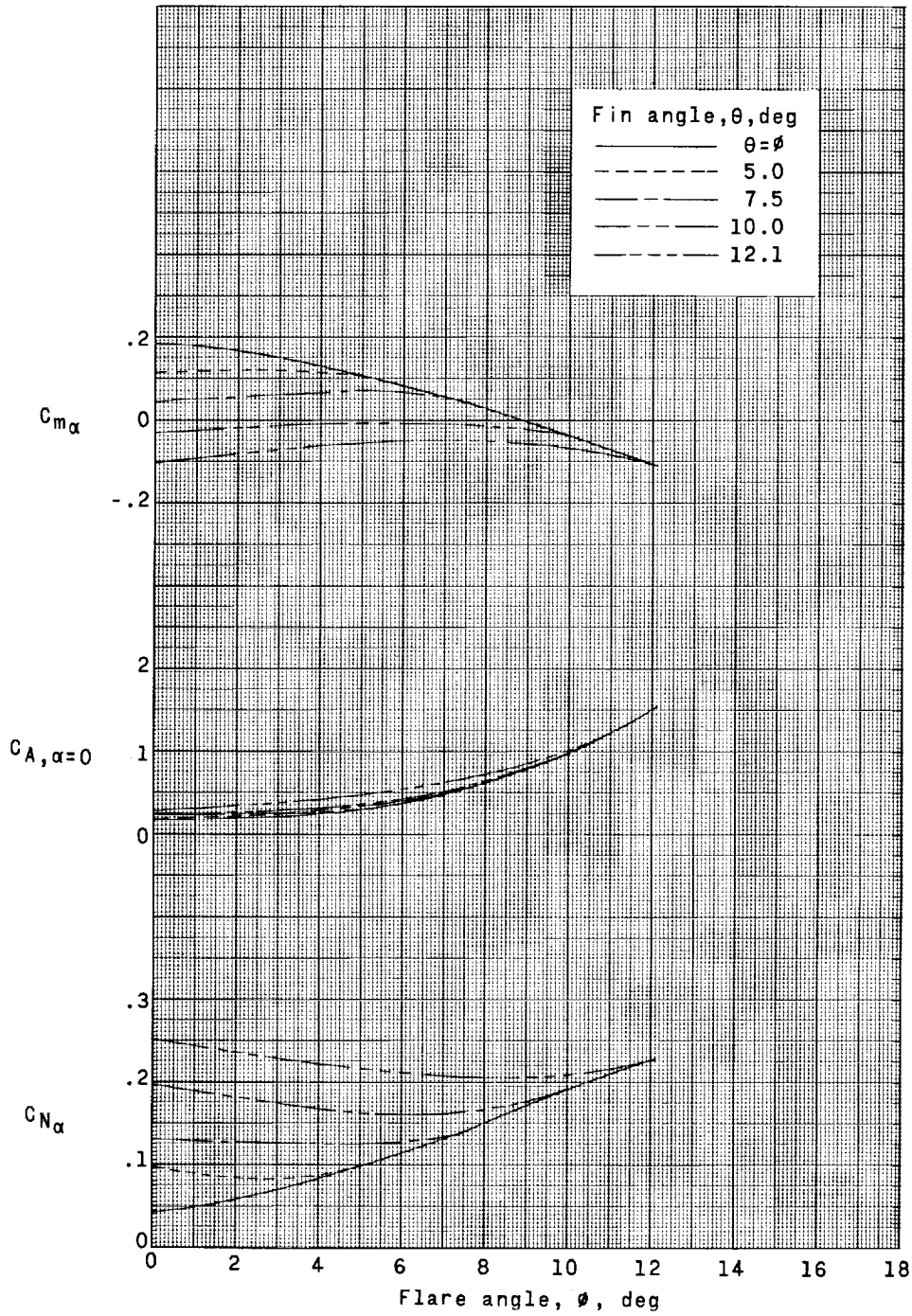

(c) Long fin-flare configurations. M = 1.61.

Figure 5.- Continued.

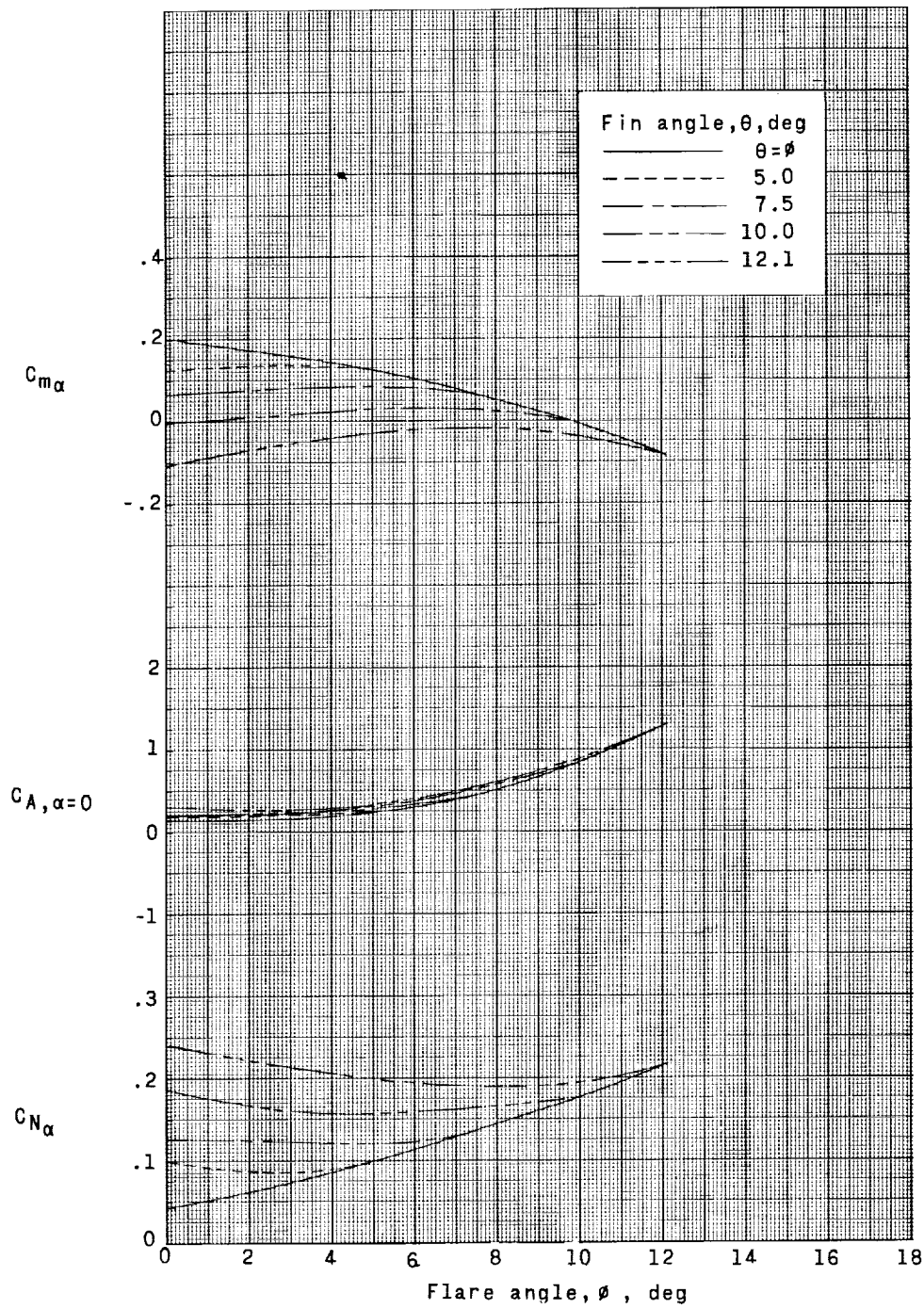

(d) Long fin-flare configurations. M = 2.20.

Figure 5.- Concluded.

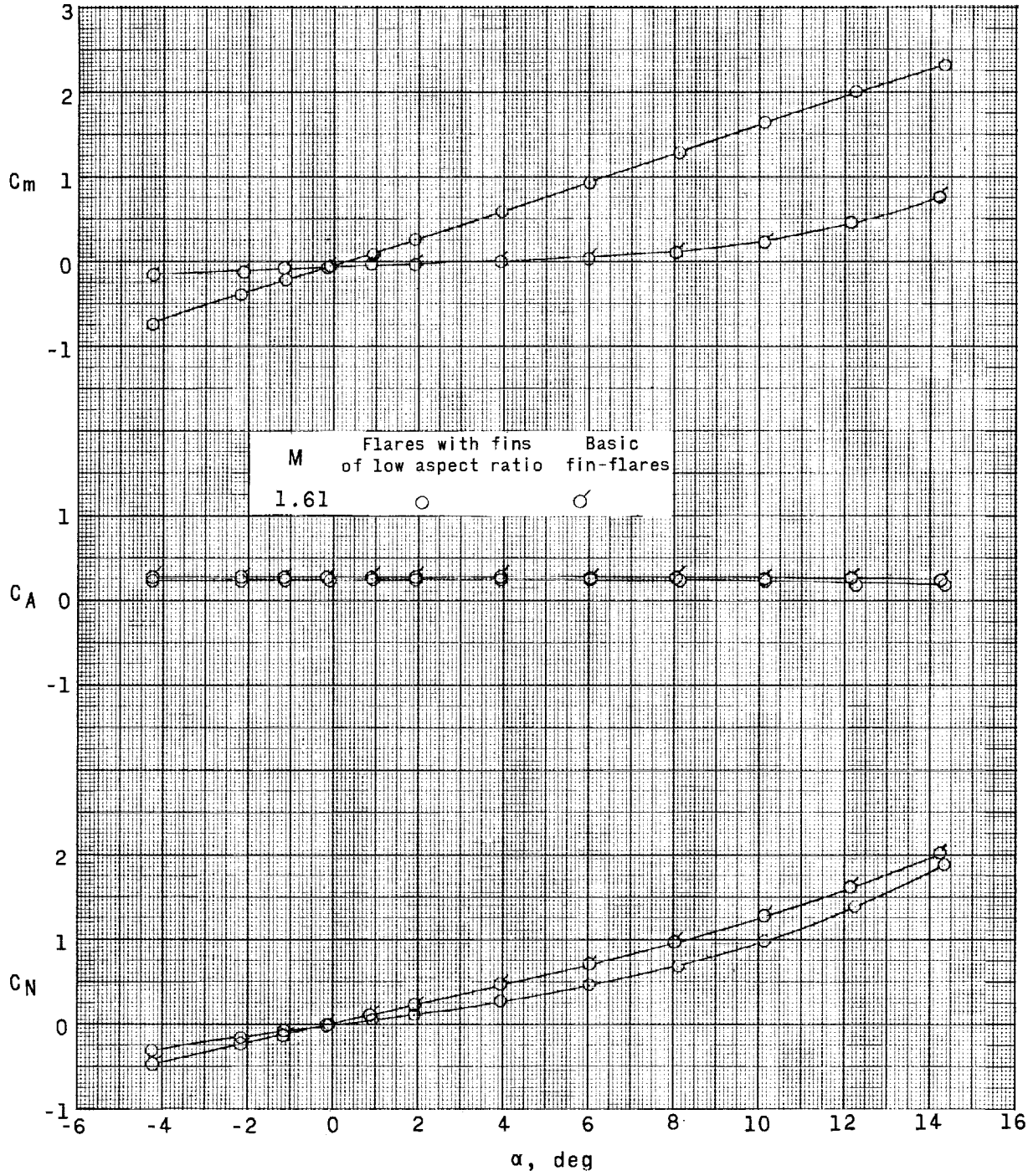

(a) Short flare (ϕ = 5°; θ = 1.28°); fin area equal to that of short fin with θ = 19.3°.

Figure 6.- Aerodynamic characteristics of fin-flare combinations with fins of low aspect ratio.

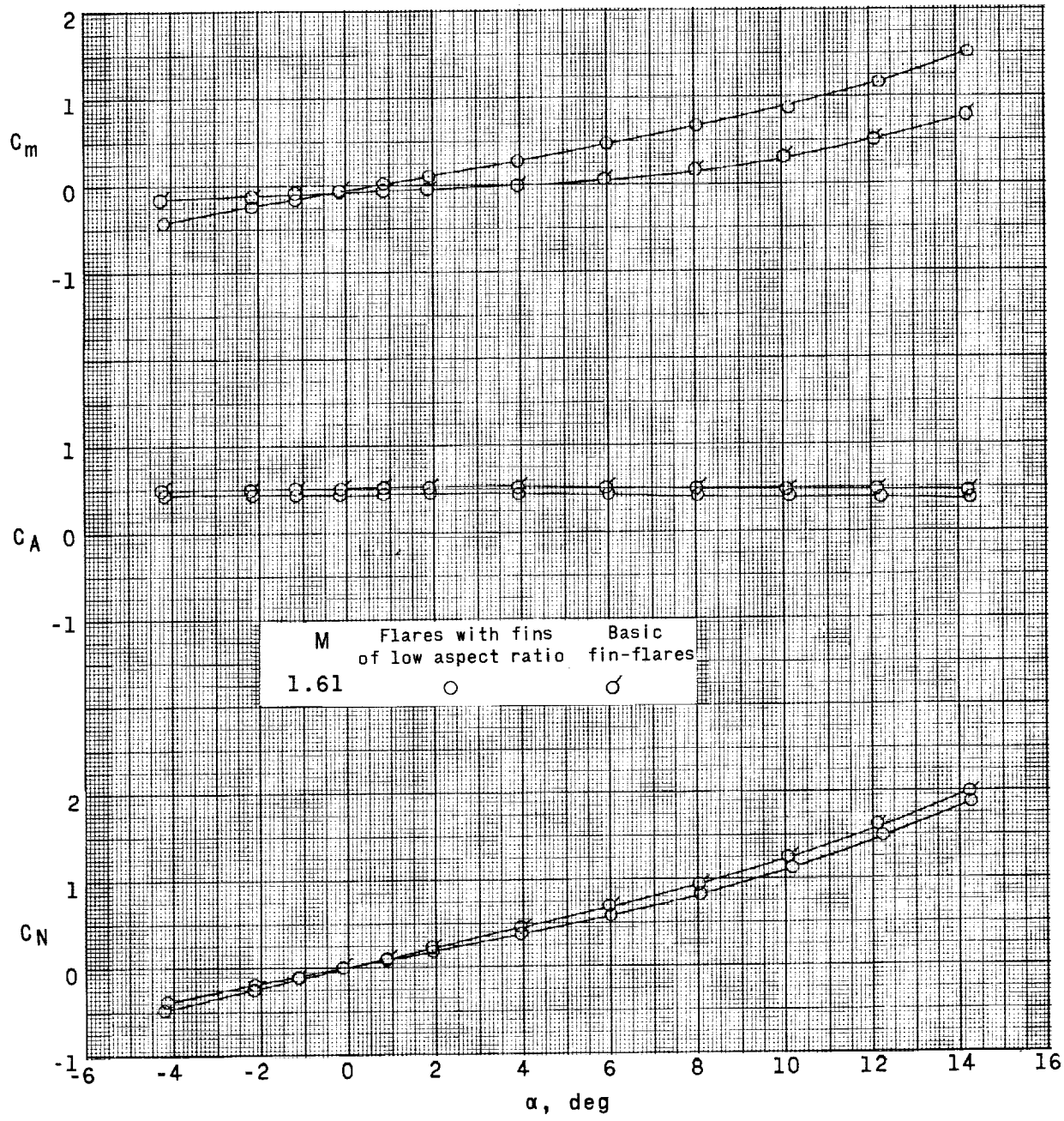

(b) Short flare (ϕ = 10°; θ = 5.03°); fin area equal to that of short fin with θ = 19.3°.

Figure 6.- Continued.

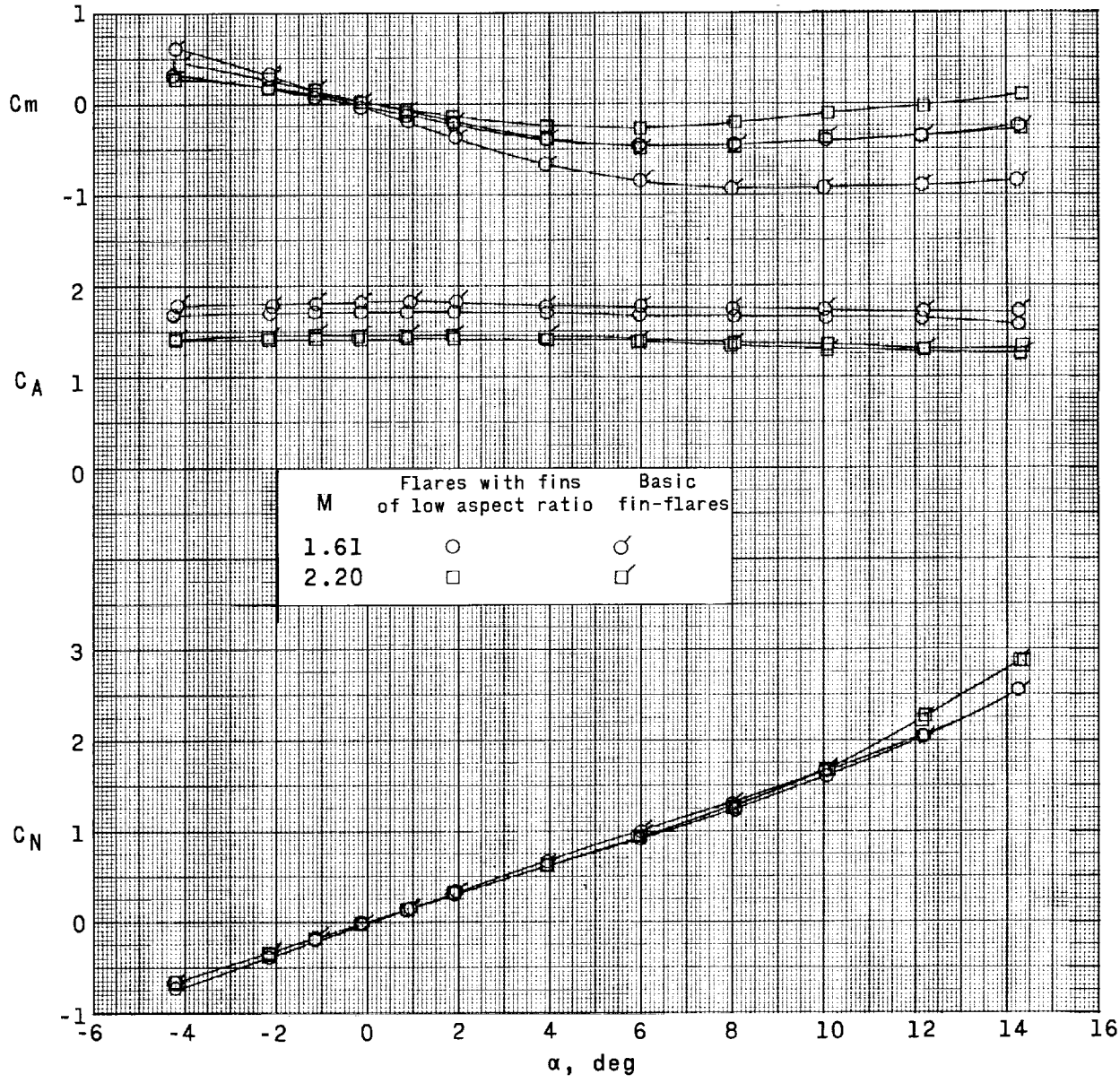

(c) Short flare (ϕ = 19.3°; θ = 13.15°); fin area equal to that of short fin with θ = 27.8°.

Figure 6.- Continued.

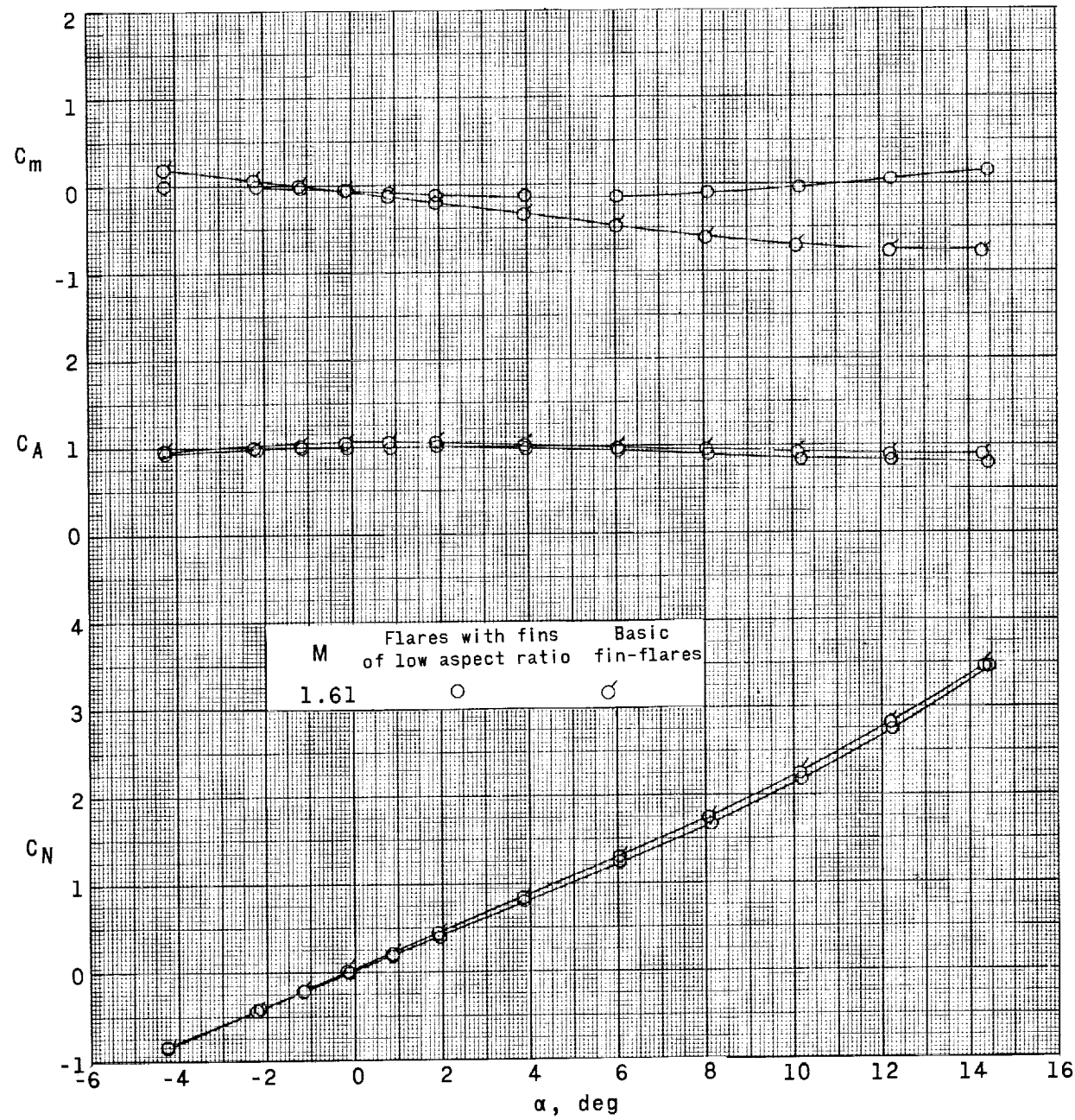

(d) Long flare (ϕ = 10°; θ = 8.32°); fin area equal to that of long fin with θ = 12.1°.

Figure 6.- Concluded.